Rationalization of the Empirical Design Method for Reinforced Bridge Deck Slab

by

Roksana Kheiri

A thesis submitted to the Faculty of Graduate Studies of
The University of Manitoba
in partial fulfillment of the requirements for the degree of
Master of Science.

Department of Civil Engineering
Price Faculty of Engineering
University of Manitoba
Winnipeg, Canada

Abstract

The empirical design of reinforced concrete bridge deck slabs of girder bridges, referred to as only 'deck slabs,' is the most efficient design method because it recognizes the inherent arching action that exists in these slabs. Because of the arching action, the deck slabs fail in a punching shear mode under much higher wheel loads than the loads that would make them fail in bending; it is noted that failure in bending assumes the absence of the arching action. The Canadian Highway Bridge Design Code provides specifications for the empirical design of deck slabs. As the term 'empirical design' implies, this method is based on experimental evidence rather than analytical methods. A computer program, PUNCH, based on an analytical method, was developed to analyze the failure loads of externally restrained deck slabs, also referred to as 'steel-free deck slabs,' which do not contain embedded reinforcement for strength. In this program, it is assumed that the transverse confinement to deck slabs is provided by steel straps lying outside the deck slabs. Thus, this program only models the behavior of externally reinforced bridge deck slabs accurately.

For internally reinforced bridge deck slabs, the stress-deformation behavior of steel in concrete is investigated in experimental evidence on concrete prisms, each with an embedded central steel bar, which has confirmed that when these prisms are subjected to tensile forces through the steel bars, the axial stiffness of the composite prisms is initially much larger than that of the bare steel bar, and decreases nonlinearly with the increase in the magnitude of tensile force. A reinforced concrete prism can thus be conceptually replaced by a hypothetical equivalent steel bar, the diameter of which is larger than that of the bare steel bar and decreases with the increase in the magnitude of the tensile force.

This thesis attempts to modify the program PUNCH to analyze deck slabs with embedded steel bars by replacing the bars with hypothetical equivalent steel bars that lie outside the concrete.

The first part of the research work involves the establishment of the changing equivalent diameter of the composite concrete prisms under gradually increasing tensile forces. This research was conducted through non-linear finite element analysis, the results of which were compared favorably with available experimental results.

The second part of the research was first to modify the PUNCH program to include variable axial stiffness of the external restraint and then to use the modified program to analyze a large number of deck slabs with variable external stiffness represented by hypothetical steel bars of varying equivalent diameters. The accuracy of the results has been established by comparing its results with those from available experimental tests, some of which were failure tests. Predictions from the modified PUNCH have confirmed that most reinforced concrete deck slabs never fail under wheel loads of even the heaviest commercial trucks traveling on highways. The modified PUNCH program is now called PUNCH.ED, can be used with confidence for predicting not only the failure loads of deck slabs but also their load-deflection behavior under smaller; loads.

Keywords:

Arching action, bridge deck slabs, empirical design, externally restrained deck slabs, FEM, rationalization

Acknowledgments:

The author wishes to thank the following:

Professor A. A. Mufti, Department of Civil Engineering University of Manitoba, under whose direction this research program was conducted.

Doctor B. Bakht, for his significant suggestions throughout this study and help in writing this thesis.

Dr. Mufti who wrote the FEMRC program, and Mr. Robert Spokowski who updated it.

Professor Mufti, Professor Newhook, and Dr. Khalid, who wrote the PUNCH program.

Research Manitoba, who provided the research grant for this investigation.

All researchers who advised the author.

To myself, who embarked on this academic journey with determination, faced challenges with resilience, and emerged with the satisfaction of accomplishment. This thesis is a proud reflection of my dedication, hard work, and commitment to personal and academic growth.

TABLE OF CONTENTS

Table of Figures

Notations:

A = $Area\ of\ the\ element$ $Eq.\ 2-1$

A_1 = $Area\ of\ the\ tire\ print$ $Fig.\ 2-9$

Ae = $Equivalent\ area\ of\ steel$ $Eq.\ 4-1$

As = $Cross-sectional\ area\ of\ steel$ $Eq.\ 2-12$

α = $Angle\ of\ shear\ crack$ $Fig.\ 2-8\ (b)$

B = $Strain\ Matrix$ $Eq.\ 2-1$

B_1 = $Diameter\ of\ equivalent\ load\ circle$ $Fig.\ 2-8\ (a)$

b = $Width\ of\ the\ section$ $Fig.\ 2-2,$

$\beta 1$ = $Rectangular\ stress\ block\ parameter$ $Eq.\ 2-15$

C = $Constant$ (= 0.7) $Eq.\ 2-11$

C_3 = $Clear\ span\ between\ girders$ $Fig.\ 2-8\ (a)$

$C1$ = $Thickness\ of\ the\ conical\ shell\ at\ its\ upper\ bounding$ $Fig.\ 2-8\ (b)$

$C2$ = $Depth\ of\ the\ compression\ rectangular\ block$ $Eq.\ 2-15$

D = $Longitudinal\ distance\ from\ the\ wheel\ load\ to\ the\ nearest\ strap$ $Fig.\ 2-9$

D_1 = $Elasticity\ matrix$ $Eq.\ 2-1$

d = $Depth\ of\ section$, depth of the slab $Fig.\ 2-2$

db = $Diameter\ of\ the\ bar$ $Eq.\ 2-9$

dbs = $Local\ bond\ slip$ $Fig.\ 2-5$

De = $Equivalent\ diameter$ $Eq.\ 4-2$

de = $Distance\ of\ steel\ bar\ and\ cracked\ concrete\ curve\ from\ the\ Y$

$axle$ $Eq.\ 4-1$

di = $Slip\ at\ the\ end\ of\ loading\ step$ $Eq.\ 2-11$

ds = $SDistance\ of\ free\ bar\ curve\ from\ the\ Y\ axle$ $Eq. 4-1$

Δ = $Vertical\ deflection$ $Fig. 2-8\ (a)$

$\Delta i{-}1$ = $The\ slip\ at\ the\ end\ of\ (i-1)\ loading\ step$ $Eq. 2-11$

Δj = $The\ slip\ at\ the\ end\ of\ loading\ increment$ $Eq. 2-11$

ΔL = Lateral displacement $Fig. 2-8\ (a)$

Δϕ = Angle of radial cracks at the side of the wedge $Fig. 2-8\ (b)$

δ = Nodal displacement vector $Eq. 2-3$

E = $Modulus\ of\ Elasticity$ $Eq. 2-12$

e = $Concrete\ strain$ $Eq. 2-6$

$E0$ = $The\ secant\ modulus$ $Eq. 2-6$

$e0$ = $Strain\ corresponding\ to\ the\ maximum\ stress\ f0$ $Eq. 2-6$

Ec = $Initial\ tangant\ modulus$ $Eq. 2-7$

ef = $Stain\ at\ failure\ stress$ $Eq. 2-6$

Es = $Modulus\ of\ elasticity\ for\ steel$ $Fig. 2-3$

Esh = $Strain\ hardening\ modulus\ of\ elasticity\ for\ steel$ $Fig. 2-3$

Et = $Tangent\ modulus$ $Eq. 2-7$

$\epsilon 0$ = $Concret\ strain\ at\ maximum\ stress$ $Fig. 2-4$

ϵf = $Maximum\ concrete\ strain$ $Fig. 2-4$

ϵs = $Yield\ strain\ of\ strap$ $Fig. 2-3$

ϵsh = $Yield\ strain\ of\ strap\ at\ strain\ hardening$ $Fig. 2-3$

f = Concrete stress $Eq. 2-6$

fc' = Maximum concrete strain $Eq. 2-7$

ff = Concrete stress at maximum strain $Eq. 2-6$

fr = Modulus of rupture of concrete $Fig. 2-4$

FW = Restraining force for the wedge $Fig. 2-8\ (b)$

h = Height of section $Fig. 2-2$

K = Stiffness $Eq. 2-12$

k = Concrete confinement constant

Ke = The element stiffness matrix $Eq. 2-1$

Kh = Non-linear horizontal spring stiffness $Eq. 2-5$

Kv = Non-linear vertical spring stiffness $Eq. 2-5$

L = Length of strap $Eq. 2-12$

Lb = Length of the bar over which spring acts $Eq. 2-9$

Mb = Number of bars in the cross-section $Eq. 2-9$

ν = Poisson's ratio $Eq. 2-2$

P = Nodal force vector $Eq. 2-3$

P_1 = Applied force $Eq. 2-13$

$R4$ = Circumferential force $Eq. 2-14$

S = Spacing of straps $Eq. 2-12$

Sg = Spacing of girders $Fig. 2-9$

Sl = Length of straps $Fig. 2-9$

Ss = Spacing of straps $Fig. 2-9$

ψ = Angle of rotation of the wedge $Eq. 2-14$

t = Thickness of the element $Eq. 2-1$

T = Compressive forces $Fig. 2-13$

θ = Inclination angle of the local axis to global axis $Eq. 2-5$

u = Horizontal node displacement $Fig. 2-1$

u (x, y) = Displacement function in x direction $Eq. 2-4$

v = Vertical node displacement $Fig. 2-1$

v (x, y) = Displacement function in Y direction $Eq. 2-4$

1- CHAPTER ONE, BRIDGE DECK SLABS AND THE REQUIREMENT FOR RATIONALIZATION

1-1 Introduction, State-of-the-Art

Reinforced concrete bridge deck slabs of girder bridges, referred to herein as only 'deck slabs,' have been widely used in North America and elsewhere in the world for more than a century. However, the design of these deck slabs based on flexural theory has remained unchanged throughout the world, except in Canada. More than 50 years ago, it was recognized in several countries of the world that deck slabs have an inherent arching action because of which the magnitude of the concentrated load under which they fail is considerably higher than predicted by the flexural theory. The recognition of the arching action considerably reduces the reinforcement requirement, which not only makes deck slabs considerably cheaper but also improves their durability. After conducting extensive experimental research, Canada took the lead in 1976 in recognizing the arching action in deck slabs and specified an empirical design method for taking advantage of the arching action. Details of this development are provided in the following.

1-2 History, Methods of Design

Composite deck slabs of girder bridges have been popular in North America since 1940 (Hewitt, 1972). A composite deck slab primarily supports and transmits the wheel loads of trucks through the girders to the substructure. There are two general methods to design bridge deck slabs: traditional and empirical. The traditional design method assumes that the deck slab fails in bending under the concentrated wheel loads, whereas the latter method uses experimental research to utilize the internal arching, because of which the deck slabs fail under wheel loads in a punching shear mode. So, the research-based empirical method results in a more economical design than that produced by the traditional method (Mufti, et al., 2008). The Canadian Highway Bridge Design Code (CHBDC) "encourages the use of empirical design method" for the design of the deck slabs (Canadian Standard Association, 2006, p. 373 C8.18.1).

1-3 Internally Reinforced Bridge Deck Slabs, Arching Mechanism, and Rationalization

As a result of an extensive experimental program at Queen's University, Kingston, Ontario, Hewitt and Batchelor (1975) "revealed the existence of a high degree of arching action in typical bridge deck slabs";

their experiments found that reinforced concrete deck slabs supported on girders failed by punching under very high wheel loads due to the compressive membrane action. As the slab under the concentrated wheel loads starts cracking midway between the girders, the neutral axis lifts, and compressive forces at the girder support induce a membrane compressive stress to the middle top of the slab. The punching failure is a result of this formed arch. The arching action takes place because of the cracking of concrete in tension. By making a rationalized approach, Hewitt investigated the required boundary conditions. A restraint factor was introduced to “quantify the boundary forces” in a computer program to predict the punching failure loads in deck slabs with typical dimensions and material properties. Based mainly on experimental work on small-scale models, a very simple empirical method of designing deck slab was introduced in the Ontario Highway Bridge Design Code (OHBDC, 1979); this method was later adopted by the CHBDC. Mufti and Bakht (2008) confirmed that a reinforced concrete bridge deck slab supported on girders and subjected to a concentrated wheel load, develops a latent arch in both the longitudinal and transverse directions. They constructed two half-scale deck slab models, one without any tensile reinforcement and the other with transverse steel straps lying below the deck slab. The deck slab without any reinforcement failed in bending with the damage covering the entire deck slab. The other deck slab with transverse steel straps connected to the top flanges of adjacent girders failed in a highly localised punching shear mode under a load that was about 2.5 times the bending failure load. Thus it was confirmed that the bottom reinforcement provides confinement and a tie for the transverse arch, and the top flange of the girders provides a tie for the arch longitudinally (Bakht, 1996); and (Canadian Standard Association, 2006, p. 374 C8.18.4.3.1).

Thus, the minimum steel reinforcement in concrete deck slabs is sufficient to carry heavy truck loads safely. Using the empirical method helps to save 35%- 40% of reinforcement in typical deck slabs. As a result of using less steel, the durability of the slab is improved, and savings regarding the maintenance cost can be considerable. The Ministry of Transportation Ontario (MTO) used the empirical design method to build a slab-on-girder bridge and tested it twice, once in 1977 and then in 1984. In 1979, the OHBDC introduced an empirical method which had the following simple requirements.

1. The bridge should have at least 3 girders.
2. The skew angle of the bridge should be less than 20^o.
3. The girder spacing should not be more than 3.7 m.
4. The concrete strength f'_c should not be less than 30 MPa.
5. The thickness of the deck slab should be the larger of 190 mm and $1/15^{th}$ of girder spacing.

6. The deck slab should contain two orthotropic meshes of steel bars, with the reinforcement ratio in each direction in each mesh being at least 0.3 %.

In later editions of the OHBDC, the minimum thickness of the deck slabs was raised to 225 mm for reasons of the durability of the deck slabs subjected to de-icing salts. In addition, following the experimental research work of Bakht and Agarwal (1995), the constraint of the skew angle of the bridge was removed by adding a requirement for composite edge beams.

1-4 Role of Reinforcement on Deck Slab Strength.

Khanna et al. (2000) studied the role of reinforcements in the strength of deck slabs through a full-scale model of a 175 mm thick composite deck that contained four sections. As shown in Figure 1.1, Section A was constructed with two layers of 15 M bars@ 300 mm, as required by the CHBDC; Section B had only the bottom steel mesh with15 M bars@ 300 mm; Section C had only the bottom transverse reinforcement with 15 M bars@ 300 mm; and Section D was reinforced by 25 mm diameter transverse Glass Fiber Reinforced Polymer (GFRP) bars @ 150 mm at the bottom of the slab. The axial stiffness of the GFRP bars in Section D was nearly the same as that of the steel bars in Section C.

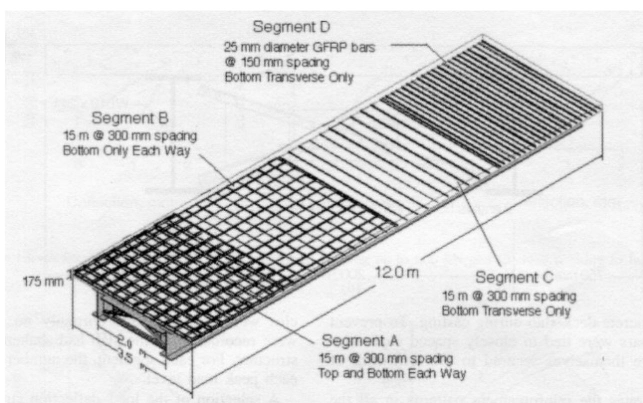

Figure 1-1 Details of a full-scale deck slab model (Khanna et al., 2000).

A photograph of the deck slab showing reinforcement in all three sections is presented in **Figure 1.2.**

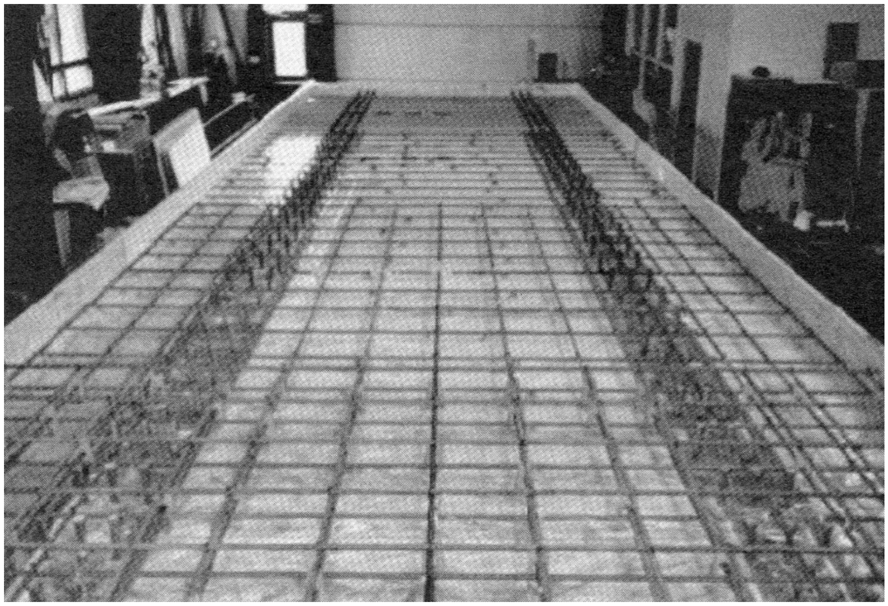

Figure 1-2 Photograph showing reinforcement in all four sections of the full-scale model of the deck slab (Khanna et al., 2000).

The four sections were tested under patch loads, representing a truck's dual tire footprint in the middle of each section. All four sections failed in punching, with Sections C and D having similar failure loads despite the GFRP reinforcement being 8.6 times stronger than the steel reinforcement. This observation leads to two important conclusions: (a) the punching shear of the deck slab depends only on its bottom transverse reinforcement, and (b) the axial stiffness of the bottom transverse reinforcement, rather than its strength, governs the failure load of the deck slab.

1-5 Externally Reinforced Bridge Deck Slabs, Arching Mechanism, and Rationalization

The durability of concrete deck slabs with embedded steel reinforcement is not good when they are subjected to de-icing salts or are in the vicinity of seawater. There are several costly measures to address the durability problem, including coated bars, thicker slabs (providing thicker cover for the steel), and increasing the density of concrete. Another way is to eliminate the source of corrosion, the steel, by replacing it with carbon or glass fibers; however, the fibers having a modulus of elasticity that is comparable to that of steel are expensive, and the inexpensive fibers have very low modulus because of which they cannot be used as tensile reinforcement.

Mufti and Bakht (2008) have shown that a deck slab can be restrained externally by steel straps; their investigation included tests on models of four deck slabs. In the first experiment, the model had polypropylene fibers mixed with concrete, and it was tested under a central patch load representing the dual-tire wheel load of a heavy truckload. The deck slab failed in a flexural mode. It was concluded that the deck did not have the required lateral resistance, so in the second experiment, end diaphragms were added to the framework. The dimensions and the concrete properties remained the same as in the first experiment. This deck slab also did not fail in a punching shear failure mode. In the third experiment, steel straps were connected to the girder's top flanges to help create the required lateral restraint. The deck slab failed in a shear punch failure under a load 2.5 times and 1.8 times larger than in the first and second experiments, respectively. Thus, it was concluded that the steel straps could provide the lateral restraint needed to develop internal arching. As mentioned, the load was at the center of the slab, so the experiment continued by loading two locations close to the transverse free edge. The failure load was 0.76 to 0.5 magnitude of the failure load at the center for the distance of 0.86 and 0.43 girder spacing from the free edge. The deck slabs with steel straps were first referred to as 'steel-free deck slabs', and later as 'externally restrained deck slabs'.

Following the experimental investigation by Mufti et al. (2008), the CHBDC provided design specifications for the cast-in-place externally restrained deck slabs, a partial cross-section of which is shown in **Figure 1.3**, along with the dimensional constraints specified by the CHBDC.

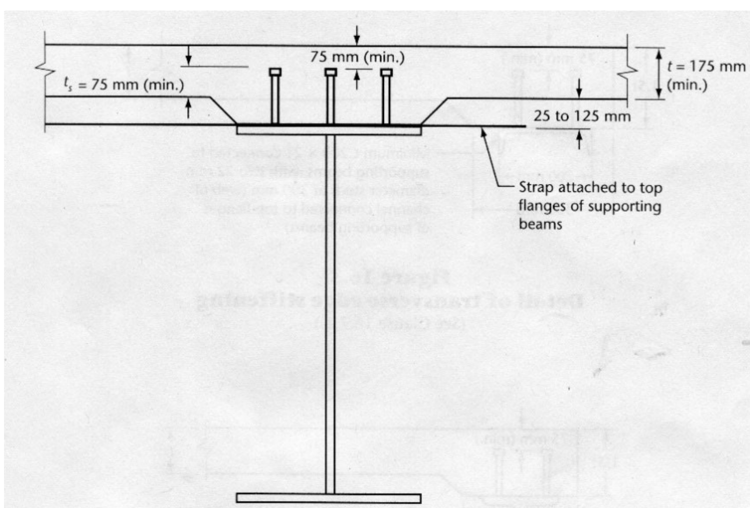

Figure 1-3 Partial cross-section of an externally restrained deck slab supported on steel girders (CHBDC, 2006).

Beside the requirements for minimum slab thickness and maximum strap spacing, the CHBDC requires that the minimum cross-sectional area of a strap, A, be as given by the following equation.

$$A = (F_S\, S^2\, S_t)/(E\, t)$$

Equation 1-1

where F_S = 6.0 MPa for external panels and 5.0 MPa for internal panels; S = girder spacing; S_t = strap spacing; E = the modulus of elasticity of strap material; and t = the thickness of the deck slab.

For crack control, the CHBDC requires an orthogonal assembly of GFRP bars placed near the bottom of the deck slab, with the cross-sectional area of the GFRP bars to be at least 0.0015 t mm^2/mm.

1-6 Application and Verification of the PUNCH Program

Mufti and Newhook (1995) have developed a computer program, PUNCH, for predicting the punching shear failure load of externally restrained deck slabs under concentrated rectangular loads; this program is described in Section 2.3. In this program, it is assumed that the transverse confinement to deck slabs is provided by steel straps lying outside the deck slabs and that the axial stiffness of the straps remains constant at all levels of loading.

1-7 Varying Axial Stiffness of Transverse Confinement

Experimental evidence on concrete prisms, each with an embedded central steel bar (Nielson, May, 1967) has confirmed that when these prisms are subjected to tensile forces applied through the steel bars, the axial stiffness of the composite prisms is initially much larger than that of the bare steel bar. It decreases non-linearly with the increase in the magnitude of tensile force. A reinforced concrete prism can thus be conceptually replaced by a hypothetical equivalent steel bar, whose diameter is larger than that of the bare steel bar and decreases with the increase in the magnitude of the tensile force.

From the above, it follows that the stiffness of the transverse confinement of reinforced concrete deck slabs varies from being largest when concrete has not cracked under low levels of applied loads to smallest when concrete is fully cracked. This is elaborated in **Figure 3-1**.

1-8 Need for Further Rationalization:

While some success has been reported in the prediction of the failure loads of reinforced concrete deck slabs by PUNCH (Mufti & Newhook, 1998) , it is unlikely that a method which cannot take account of the varying stiffness of the transverse confinement can predict accurately the behaviour of these deck slabs at all levels of loading. It is important to note that the failure load of deck slabs, being much larger than actual wheel loads, never governs the design of deck slabs. To evaluate the load-carrying capacity of existing deck slabs, the failure load is considered for deck slabs in which severe deterioration has reduced their effective thickness of the deck slab significantly.

An analytical method for predicting the load-deflection behavior of reinforced concrete deck slabs should be able to deal with the varying axial stiffness of the transverse confinement. In this thesis, a method is developed to replace the bottom transverse bars in the reinforced concrete deck slabs with hypothetical steel bars, the equivalent diameters of which change with the loading level. The program PUNCH is modified to take account of the varying axial stiffness of the transverse confinement. The modified program is called PUNCH-ED, with 'ED' referring to 'empirical design.'

2- CHAPTER TWO, COMPUTER PROGRAMS

2-1 General

The two programs FEMRC and PUNCH used in this thesis, are discussed in this chapter along with the details of their formulation.

2-2 The FEM and FEMRC

Finite Element Analysis (FEA) divides a complex structure into smaller elements and solves the partial differential equations using numerical methods. The elements are connected at nodes and form a mesh. The behavior of each element is analyzed and the structure is then analyzed based on that.
(Nielson, May, 1967)describes the main steps of FEM analysis.

- Idealization: discretization is the process of dividing the entire structure into discrete finite elements. The structure is divided into minimal parts as elements. The elements can be in the form of a triangle, rectangle, or any other shape, and the shapes have nodal points connected to them at element corners. The forces are applied through the nodes, and displacement is calculated at the nodes.

- Determination of element stiffness: An element's stiffness matrix represents its stiffness characteristics. The stiffness matrix relates the nodal displacement to the applied nodal forces. The deformations and stresses throughout the structure are solved using the global stiffness matrix for the nodal displacements. The stress-strain and equilibrium equations are defined, and the connection between nodal displacement values and the applied loads is established (Lyu, 2022).

- Application of the boundary conditions: the constraints on the structure are represented in the form of displacement or forces.

- Solution of the equations: by the application of iterative method techniques the system of equations is solved to determine the nodal values and find the structure’s response to the applied loads and boundary conditions.

- Determining element stresses: the behavior of the structure is determined by extracting information about stress distribution and deformation.

There are four assumptions in the FEA (Lyu, 2022):

(a) Continuum: the stresses and strains are continuous. This is not valid for non-linear FEA.

(b) Linear elasticity: the elastic parameters of materials are constant. This is not valid for non-linear FEA.

(c) Small deformation: the deformations in the body are much smaller than their size and do not change the dimensions.

Additional assumption of isotropy and homogeneity for linear FEA: the mechanical behavior of a material is similar in different directions and all parts of it.

The FEMRC program used in the thesis of (Nielson, May, 1967) had elements with a rectangular shape and the nodes having two degrees of freedom. This selection is because of differences between the triangular and rectangular elements. The strain remains constant within the element in triangular elements. In linear triangular elements with three nodes, the interpolation functions representing displacements or strains result in constant strain within the element. This characteristic is known as a "linear strain triangle" or "constant strain triangle." While this simplifies the mathematics, it can lead to a less accurate representation of deformation in certain situations, especially when dealing with large deformations or nonlinear material behavior. The accuracy of a rectangular element with four nodes is one degree higher than that of a triangular element with three nodes. The use of higher-order interpolation functions in rectangular elements allows them to capture variations in areas of high-stress rises better. This is crucial for accurately predicting the behavior of structures in nonlinear situations (Lyu, 2022). Also, Mufti et al. (1970) suggested that in the investigation of the behavior of reinforced concrete elements using FEM applying quadrilateral elements will improve the crack pattern and will represent the stress field more effectively. The element used in FEMRC is shown *in* ***Figure 2-1***.

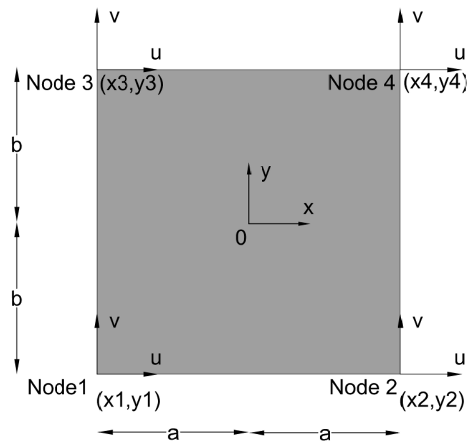

Figure 2-1 The rectangular element in a finite element model

In the FEMRC program, the load increases monotonically, and the stresses and strains at each loading step are added to calculate the final strain and stress in any element. Also, the material is non-linear; however, this non-linearity can be created within the stiffness matrix regarding the constitutive relationships or criteria of failure (Spokowski, May 1972, p. 8).

2-2-1 Global Stiffness Matrix for Steel and Concrete:

According to Spokowski May (1972), concrete is a non-homogenous material with non-linear behavior. This non-linearity can be defined using "piecewise linear analysis," an approximation using linear segments. For an eight-degree-of-freedom plane stress rectangular element, the element stiffness matrix is as defined by *Equation 2-1* (Lyu, 2022):

$$K^e = \int_{A^e} B^T \underset{1}{D} B dA.t = \begin{bmatrix} k_{11} & & & \\ k_{21} & k_{22} & sym & \\ k_{31} & k_{32} & k_{33} & \\ k_{41} & k_{42} & k_{43} & k_{44} \end{bmatrix}$$

Equation 2-1

Where,

K^e is the element stiffness matrix for a 4 x 4 rectangular element;

A is the area of the element;

t is the thickness of the element;

D is the elasticity matrix (Lyu, 2022); and

B is the differential operator or strain shape function;

$$D = \frac{E}{(1-\nu^2)} \begin{bmatrix} 1 & \nu & 0 \\ \nu & 1 & 0 \\ 0 & 0 & \frac{1-\nu}{2} \end{bmatrix}$$

Equation 2-2

In *Equation 2-2,* E is Young's modulus, and v is the Poisson's ratio. For isotropic material, the properties are equal in the x and y directions. Both steel and concrete are isotropic (Spokowski, May 1972).

The minimum potential energy theorem is:

$$P = K\delta$$

Equation 2-3

P is the nodal force vector, K is expressed in ***Equation 2-1***, and δ is the nodal displacement vector.

The strain matrix can be derived using displacement functions (Lyu, 2022):

$$\begin{cases} u\,(x,y) = a_0 + a_1 x + a_2 y + a_3 xy \\ v\,(x,y) = b_0 + b_1 x + b_2 y + b_3 xy \end{cases}$$

Equation 2-4

The elastic module is kept equal and depends on the largest principal strain at the centroid of a particular finite element, implying that the material's response is influenced by the dominant strain direction within the element. It is acknowledged that the stress-strain curves are non-linear, which needs to be considered in the analysis. Tangent moduli are changed at each loading increment to account for non-linear behavior in stress-strain curves. The state of strain influences the decision to change these moduli at the centroid of the finite element (Spokowski, May 1972, p. 10).

In a stiffness matrix of a reinforced concrete member, concrete and steel can be treated separately concerning degrees of freedom while they occupy the same positions in space. To simplify the integration of the steel reinforcement into the finite element model with two dimensions, the circular cross-sections of the steel bars embedded in the concrete are converted into a transformed section with a rectangular cross-section **Figure2-2.** (Spokowski, May 1972, p. 10).

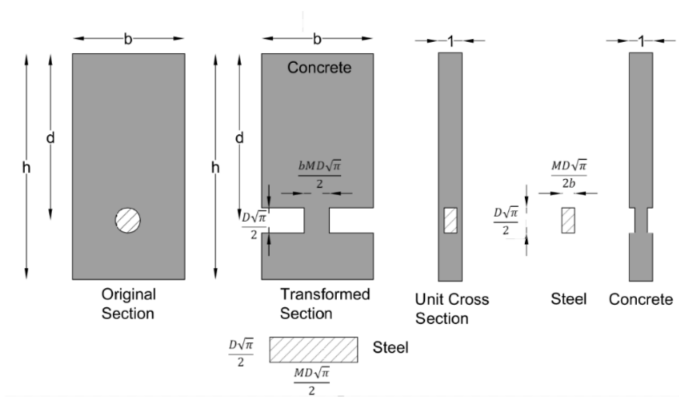

Figure 2-2 *The transformed section and the unit cross-section*

In ***Figure 2-2,*** M is the number of bars if more than 1, and D is the diameter of bars.

2-2-2 Global Stiffness Matrix for Bond:

The bond between concrete and steel is modeled using four-degree-of-freedom spring linkages to represent the force-slip relationship at the steel-concrete interface. This allows for the inclusion of the interface behavior in numerical simulations, providing a compromise between accuracy and computational efficiency. The corresponding nodes on concrete and steel connect with the spring linkages. The stiffness matrix for these springs is:

$$K = \begin{bmatrix} -\cos\theta & \sin\theta \\ -\sin\theta & -\cos\theta \\ \cos\theta & -\sin\theta \\ \sin\theta & \cos\theta \end{bmatrix} \begin{bmatrix} K_h & 0 \\ 0 & K_v \end{bmatrix} \begin{bmatrix} -\cos\theta & -\sin\theta & \cos\theta & \sin\theta \\ \sin\theta & -\cos\theta & -\sin\theta & \cos\theta \end{bmatrix}$$

Equation 2-5

where θ is the inclination angle of the local axis to the global x-axis, K_h and K_v are non-linear horizontal and vertical spring stiffness that must be calculated at each incremental loading step.

2-2-3 Failure Criteria in Steel

The criteria for determining steel failure rely on the stress-strain curve as a reference. The principal strains within the elements are compared to this curve to establish an appropriate value for the tangent modulus. If the principal strain in any steel element surpasses the yield strain, a nominal value (0.06894757 Mpa.) is assigned to the tangent modulus in the elasticity matrix. A practical approach is taken to avoid potential issues with a malfunctioning stiffness matrix due to many yielded elements. Typically, only one or two elements are yielded in each loading step. Similarly, if the principal strain exceeds the strain hardening limit, the initial strain hardening modulus is applied in the stress matrix. It's important to note that this analysis does not account for further steel deformations (Spokowski, May 1972). The stress-strain curve for steel is shown *in **Figure 2-3***.

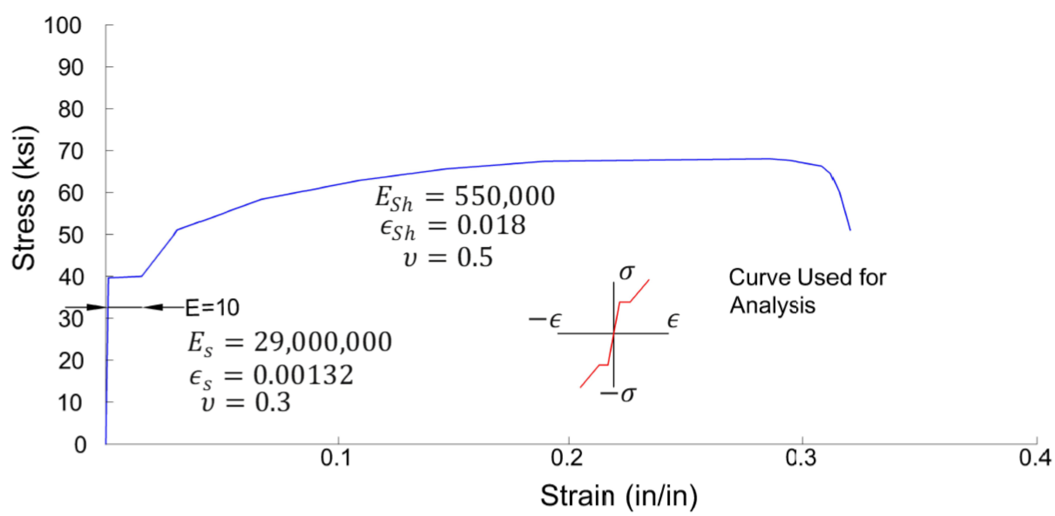

Figure 2-3 The strain-stress curve for 40 ksi steel grade (Spokowski, May 1972).

2-2-4 Failure Criteria in Concrete

The methodology employed to characterize concrete elements' structural response closely resembles the steel elements' approach. The concrete stress-strain curve is utilized to ascertain the tangent modulus incorporated into the elasticity matrix. Furthermore, well-defined failure criteria are employed to establish the structural capacity of each concrete element. The concrete stress-strain curve is typically represented using Saenz's equation (Nielson) (Spokowski, May 1972).

$$f = \frac{E_e}{1 + (R + R_E - 2)\frac{e}{e_0} - (2R - 1)\left(\frac{e}{e_0}\right)^2 + R\left(\frac{e}{e_0}\right)^3}$$

Equation 2-6

Where,

$$R = \frac{R_E(R_f - 1)}{(R_e - 1)^2} - \frac{1}{R_e}$$

$$R_E = \frac{E_c}{E_0}$$

$$R_f = \frac{f_c^{'}}{f_f}$$

$$R_e = \frac{e_f}{e_0}$$

$$E_0 = \frac{2f_c^{'}}{e_0}$$

In the above equations, f is concrete stress, e is concrete strain, e_0 concrete strain corresponding to maximum stress, $f_c'$is maximum concrete strain, e_f is maximum concrete strain at failure, E_c is initial tangent modulus, E_0secant modulus (Nielson) (Spokowski, May 1972).

Differentiating *Equation 2-6* concerning e results in the tangent modulus expression for uniaxial compression (Nielson, May, 1967, P.55.):

$$E_t = \frac{df}{de} = \frac{E_c(1 + C_1\left(\frac{e}{e_0}\right)^2 - 2C_2\left(\frac{e}{e_0}\right)^3}{(1 + C_3\left(\frac{e}{e_0}\right) - C_1\left(\frac{e}{e_0}\right)^2 + C_2\left(\frac{e}{e_0}\right)^3)^2}$$

Equation 2-7

Where,

$C_1 = 2R - 1,$

$C_2 = R,$

$C_3 = R + R_E - 2$

The tangent modulus defined as shown above will be used as a basis for the next increment. The initial tangent modulus is used for the concrete in uniaxial tension in which the maximum principal strains are positive because they will have linear behavior up to failure (Spokowski, May 1972, p. 15) (Nielson, p. 55). The stress-strain curves used by Nielson and Saenz are shown in ***Figure 2-4***.

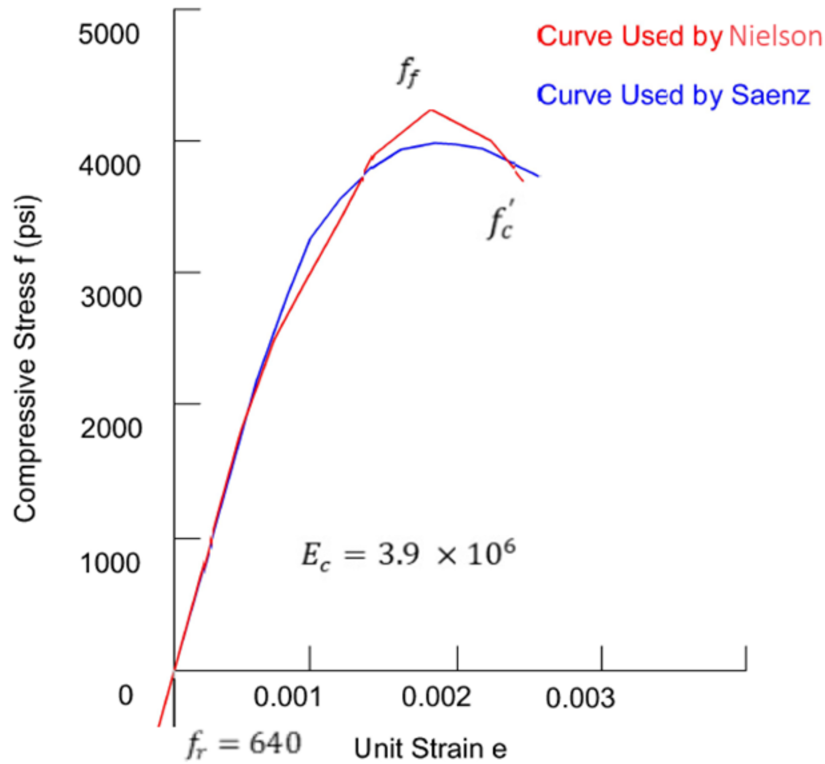

Figure 2-4 Strain- stress curve for concrete (Spokowski, May 1972) & (Nielson, May, 1967)

Tension failure occurs when the principal stresses reach the modulus of rupture at the centroid, resulting in the zero thickness being set for the element. In a compression state, if the principal compressive strains exceed the maximum permissible concrete strain. The forces on the nodes of the failed element will be transferred to the nodes of the next element (Spokowski, May 1972, p. 16).

2-2-5 Failure Criteria in Bond

The spring constant is defined by K_h and $K_{v,}$ which are determined by load-deformation assessment for both pullout and dowel actions, respectively. Realistic values of pullout stiffness K_h depend on the bar type and spacing, concrete type, and the thickness of the cover and can be estimated using pullout tests. However, Nielson introduced a non-linear equation to calculate the pullout spring constant (Spokowski, May 1972).

The local bond-slip d_{bs} (x 10^{-6} inches) are inputs to calculate the local bond stress u_{bs} (psi).

$$u_{bs} = 3606 \times 10^3 d_{bs} - 5356 \times 10^6 d_{bs}^2 + 1986 \times 10^9 d_{bs}^3$$

Equation 2-8

Figure 2-5 shows the local bond-slip curve. At any point, the slope of the tangent to the curve is K_h.

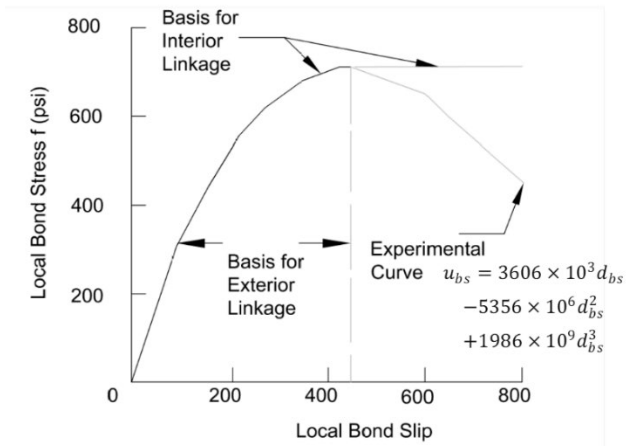

Figure 2-5 Bond-slip curve (Nielson) & (Spokowski, May 1972)

From the bond-slip equation:

$$K_h = \frac{du_{bs}}{dd_{bs}} M_b L_b \pi d_b$$

Equation 2-9

M_b is the number of bars in the cross-section, L_b is the length over which the spring acts or bar linkage spacing, and d_b is the diameter of the bar. The curve results from an internally instrumented bar pullout test by Bresler and Bertero, from which Nielson could derive *Equation 2-9*.

The steel elements are connected to concrete elements with a spring element resembling bond linkage at the top and bottom of the bar element, as illustrated *in* ***Figure 2-6***.

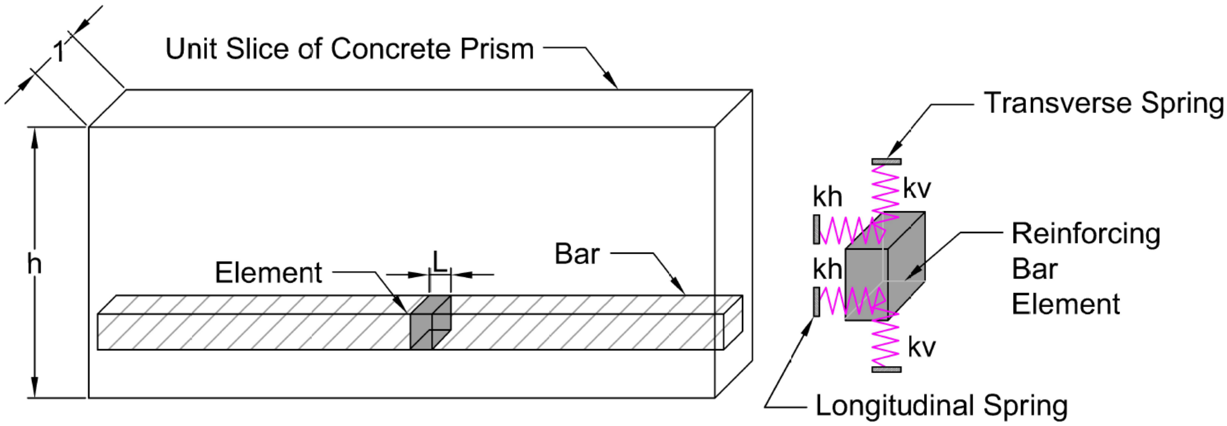

Figure 2-6 The steel element inside the concrete and the linkage elements connected to the nodes.

For the spring constant $K_{v,}$, the linkage element perpendicular to the reinforcing bar, the experimental research shows that this value is relevant to the initial tangent modulus of concrete and depends on the number and diameter of bars and the element's width.

$$K_v = \frac{E_c M_b d_b L_b}{b}$$

Equation 2-10

In which E_c is the initial tangent modulus of concrete, $M_b$is the number of bars, d_b is the diameter of bars, $L_b$is the element's width or the length that springs acts over (Spokowski, May 1972, p. 20). When the bond slips more than 449×10^{-6}inches, K_h becomes negative. For the spring elements at the exterior or open face of the concrete, once the slip value passes the slip limit, the bond stress will become zero, and the linkage element is considered broken. Nielson defines the exterior spring element to be at a distance of "one and one-half bar diameter" from the open face of the concrete. Conversely, the interior elements will have the constant bar stress equal to the slip limit (Mufti, et al., 1970, p. 11 & 12).

2-2-6 Incremental Loading:

In the first load increment, the initial modulus of elasticity E is used, and the stiffness of the spring elements is the initial slope of the non-linear stress-slip curve presented by Nielson. Then, the global stiffness matrix is formed and inverted, leading to the solution of equilibrium equations for calculating displacements, resulting in the calculation of stress and strain at the center of concrete and steel elements and bond forces. Then, a comparison with the failure criteria is done to check if the concrete principal stresses pass the modulus of rupture or if the slip passes the defined slippage value. Further on, the strain level in the previous step is used to calculate the stiffness of the concrete element. The stiffness of the steel will only be affected if it passes the yield point. The slip is calculated as follows:

$$d_i = \sum_{j=1}^{i-1} \Delta_j + c\Delta_{i-1}$$

Equation 2-11

$Increment\ \Delta_j$ is the slip, or the relative nodal displacement at the end of the loading increments j, $\Delta_{i-1}$is the slip at the end of the (i-1) loading step, C is the constant equal to 0.7 (Spokowski, May 1972, p. 19) (Mufti, et al., 1970, p. 11). Again, a global stiffness matrix is compiled by the changed element stiffness and the loop of finding displacement, stresses, and strains and checking for concrete tensile cracking and bond breakage repeats.

The general FEM was discussed in brief, and the conceptual theory of the FEMRC program is explained so far. The program takes inputs for the idealization consisting of node and element numbers, nodal coordinates, element parameters, boundary conditions, the initial properties of the material, initial loads, incremental loads, and the number of increments, degree of freedom for each node, stress-strain curve constants for steel and concrete.

The program gives the following as the output: a print of the input data, stiffness values for spring elements, residual values, the displacement for each node in X and Y directions, the stress and strain at the center of each element with the corresponding modulus of elasticity, bond force, stress, and the displacement for the spring elements are also given.

2-3 The Theory of Punching Shear in Bridge Deck Slabs and the Derived Equations

In the program PUNCH, Newhook and Mufti (1995) have included a method for predicting the punching shear failure of laterally restrained fiber-reinforced deck slabs. In their formulation, they have used the theory developed by (Kinuenen & Nylander, 1969) , who have suggested that when the concentrated load is applied to a concrete deck slab, radial cracks originate from underneath the load at the bottom of the slab. As the load increases, these cracks progress to the top to create circular cracks with a diameter approximately the same size as the girder spacing. Also, at loads smaller than the failure load, a shear crack is a circumferential crack at some distance from the load, and as the load increases, the cracks progress to the surface and form a punched cone. There are radial and circular cracks on the surface, so the concrete outside the punched cone can be divided into wedges (Mufti & Newhook, 1998). Studying the free body diagram of the wedge, $(\Delta\phi)$of the circle, and the cone resulted in the mathematical equations and an algorithm used to develop the PUNCH program. Newhook and Mufti (1995) calculated the punching load for a half-scaled deck slab, a skew deck slab, and a full-scale deck slab using the PUNCH program. They compared the results to the experimental results, showing that the punching load-bearing capacity for the externally restrained, fiber-reinforced concrete, and slab-on-grade slabs can be accurately predicted using the PUNCH program. The fibers mixed with concrete required for crack control do not have significant contribution to the strength of concrete. They also showed that the critical parameters in this calculation are the girder spacing, slab thickness, strap stiffness, concrete strength parameter, and the area of the load patch. The loading area in Kinnunen and Nylander's method is circular, so Newhook and Mufti used the equivalent circle with diameter B in the equations and the PUNCH program (Mufti & Newhook, 1998). The affecting parameters are explained later.

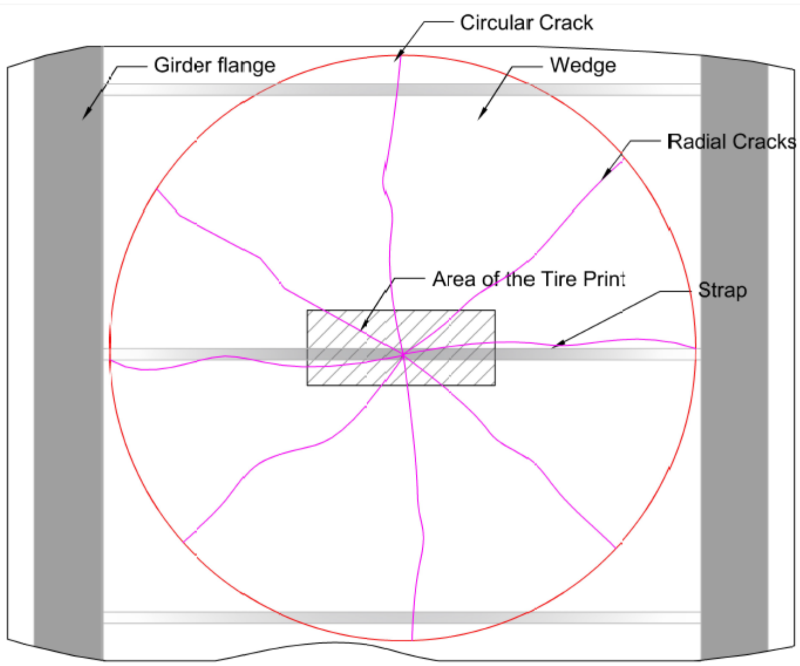

Figure 2-7 The cracks observed at the surface of a bridge deck slab failed in shear punching (Mufti, et al., 2008)

As shown in ***Figure 2-7***, a "conical shell of high compressive stress" is formed where the wedge intersects the loaded zone, which helps transfer the vertical vehicle loads to the compressive membrane forces. This compressive force (T) is perpendicular to the wedge, making an angle of α with the horizontal direction; the wedge rotates with an angle of ψ thus, the (T) has vertical and horizontal components. In the horizontal direction, another force is formed due to the lateral restriction in response to the lateral displacement of the strap (F_w). This parameter depends on the stiffness K defined as:

$$K = \frac{E.A_s}{\frac{L}{2}.S}$$

Equation 2-12

In which S is the strap spacing, and L/2 is equal to $C_3/2$, as shown in ***Figure 2-8*** (a).

There is a tangential compressive force with a resultant ***Figure 2-8 (***b). The span between the girders is C, and lateral displacement at the strap is $\Delta_L = \psi\,(d - y)$, and the vertical deflection is $\Delta = \psi\,\left(\frac{C}{2}\right)$, the center of rotation is located at a distance y under the center of the loading, as illustrated in ***Figure 2-8*** (a)

.

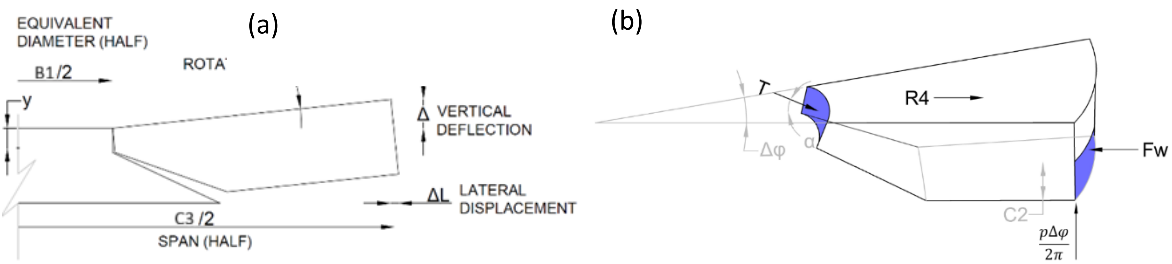

Figure 2-8 (a) half of the deck slab and the rotated part after cracking with the related deflections, angles, and dimensions, (b) an individual wedge of concrete showing restraining and compression stresses and the resultant forces.

So, the three equilibrium equations drive (Mufti, et al., n.d.):

On the vertical direction from the equilibrium of the applied vertical force P_1 and the vertical component of T,

$$T = \frac{P\Delta\phi}{2\pi\sin(\alpha - \psi)}$$

Equation 2-13

On the horizontal direction from the equilibrium of the restraining forces F_w and the horizontal component of,

$$\frac{P_1}{2\pi}\cot(\alpha - \psi) + R_4 = \frac{C_3}{K}\psi(d - y)$$

Equation 2-14

In which R_4 is the tangential compressive force resultant.

Taking the equilibrium of moments around the center of rotation,

$$R_4\left(d-\frac{y}{3}-\frac{C_2}{2}\right)+\frac{P_1}{2\pi}\cot(\alpha-\psi)\left[d-\frac{\beta_1 y}{2}-\frac{C_2}{2}-\psi\left(\frac{C_3}{2}-\frac{B_1}{2}\right)\right]=\frac{P_1}{2\pi}\left[\frac{C}{2}-\frac{B_1}{2}+\psi\left(d-\frac{\beta_1 y}{2}-C_2\right)\right]$$

Equation 2-15

In the equations above β_1 is the rectangular stress block parameter, and C_2 is the depth of the compression rectangular block on which restraining stresses are affected (Newhook, 1997, p. 23). The other notation is defined as follows.

- S_g, spacing of girders,
- S_l, length of the strap (clear distance between girder flanges),
- A_1, area of the tire print,
- S_s, spacing of the straps, d depth of the concrete (depth of concrete plus the haunch over the girders),
- E, modulus of elasticity of steel straps,
- f_c', compressive strength of concrete,
- β_1, rectangular stress block parameters

$$\beta_1 = 0.85\ for\ f_c' \leq 30\ MPa$$

$$\beta_1 = 0.85 - \frac{(f_c' - 30)}{10}\quad 30\ MPa < f_c' \leq 55\ MPa$$

$$\beta_1 = 0.65\ for\ f_c' \geq 55 MPa$$

- K, transverse restraint stiffness, *Equation 2-12*
- K, concrete confinement constant (in the absence of data, it can be taken as 10),
- ϵ_y, yield strain of strap,
- B_1, the diameter of the equivalent circle for the loaded area,

$$B_1 = 2(b + w)/\pi$$

- D, longitudinal distance from the wheel load to the nearest strap,
- A_s, an area of the strap (Mufti, et al., 2008).

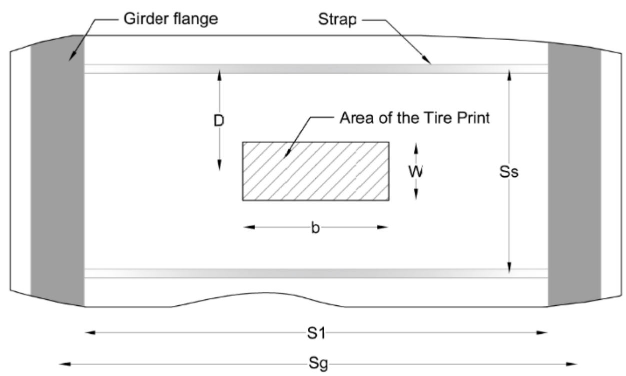

Figure 2-9 Defined geometrical parameters in PUNCH.

The geometrical parameters used in PUNCH are illustrated in ***Figure 2-9***. *PUNCH considered the S1 as the distance between the girders as the distance affected by the load so as per* ***Figure 2-7*** *the diameter of the crack is equal to the girder spacing.*

2-4 Conclusions:

-The FEMRC is a program based on FEA,

-FEMRC can model the interaction and bond between concrete and steel by simulating the bond as spring elements with stiffness located on each node in the same direction as the corresponding degree of freedom.

-FEMRC can calculate the stresses associated with each element, whether rectangular or spring elements, and can calculate the relative strain, deflection, and failure punch load.

-The PUNCH program is based on the equilibrium of forces affecting a concrete wedge formed by the cracks when normal loads are applied to an externally reinforced concrete bridge deck slab and failure happens in the punch mode.

3- CHAPTER THREE, REINFORCED CONCRETE PRISMS IN TENSION

3-1 General

Nielson tested several concrete prisms, each a steel bar placed eccentrically or at the centre of the prism. Each prism was tested under a gradually increasing tensile force applied to the steel bar. The observed stress-displacement curve for one of the prisms is presented in ***Figure 3-1***, along with corresponding curves for the bare steel bar and a transformed section in which it is assumed that concrete does not crack. It can be seen in this figure that the observed behaviour is close to that of the transformed section under initial stages of loading. Under higher loads, the actual behaviour is closer to that of the bare steel bar. This observation clearly shows that under initial stages of loading when concrete has not cracked, the composite prism behaves like the transformed section. When it is fully cracked at higher loads, concrete does not contribute to the axial stiffness of the reinforced prism.

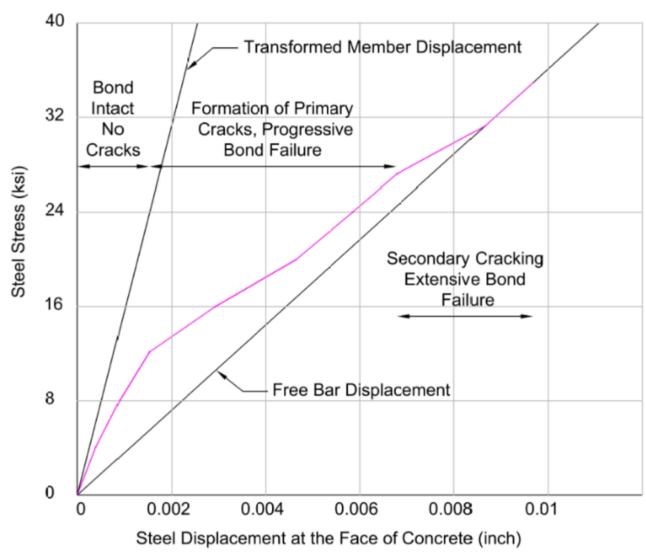

Figure 3-1 Eccentric Tensile Specimen Steel Displacement (Nielson, p. 153)

Nielson applied the FEA for reinforced concrete prism with incremental loading to model and investigate the progressive cracking and local bond failure. The model allowed for non-homogeneity and non-linearity in the bond by using spring linkage elements and non-linearity in the material properties. He compared the analysis results with experimental data, and concluded that the stresses in concrete and steel, displacement, location of cracks, extent of the cracks, and width matched the observed data (Nielson, p. 156). The Nielson results are used in this thesis to validate the predictions of the computer program FEMRC.

3-2 Idealizations and Modeling

Details of one of the reinforced prisms tested by (Nielson, May, 1967) and its idealization are shown in ***Figure 3-1***.

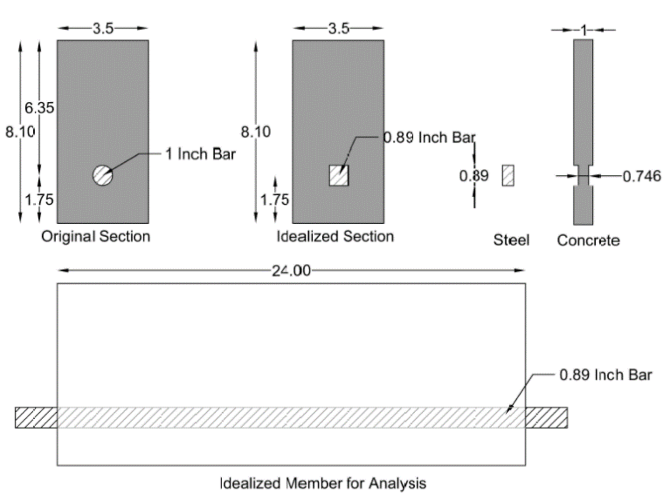

Figure 3-2 Details of one of the models tested by Nielson and its idealisation (Nielson, p. 133) *(All dimensions in inches).*

The width of the steel in the unit section is calculated as follows:

$$S = \frac{mD\sqrt{\pi}}{2b} = \frac{1 \times 1\sqrt{\pi}}{2 \times 3.5} = 0.254\ inch$$

The section of the concrete at the level of the reinforcement will have the thickness of:

$$1 - S = 0.746\ inch$$

Nielson mentioned that the accuracy of the FEM depends on grid refinement, the shape of the elements, and the validity of the assumptions (Nielson, p. 157). Meanwhile, Nielson claimed the possibility of achieving accurate results with coarse mesh idealization in the case of a higher-order shape function (Nielson, p. 157). Nielson used triangular elements. However, rectangular elements are used in modeling for this study. Rectangular elements have more nodes and more degrees of freedom; thus, they have higher order compared to the elements that Nielson used. Nielson also noted that, given an element type, more accurate results can be gained by refining the mesh (Nielson, p. 157). As a result, three different idealizations will be tested in this study with respect to the eccentric prism of Nielson reinforced with a single steel bar. These three idealizations differ in the element size and aspect ratio.

The first idealization uses a crude meshing system with only nine elements; as shown in ***Figure 3-3***, the elements have an aspect ratio varying from 0.21 to 6.

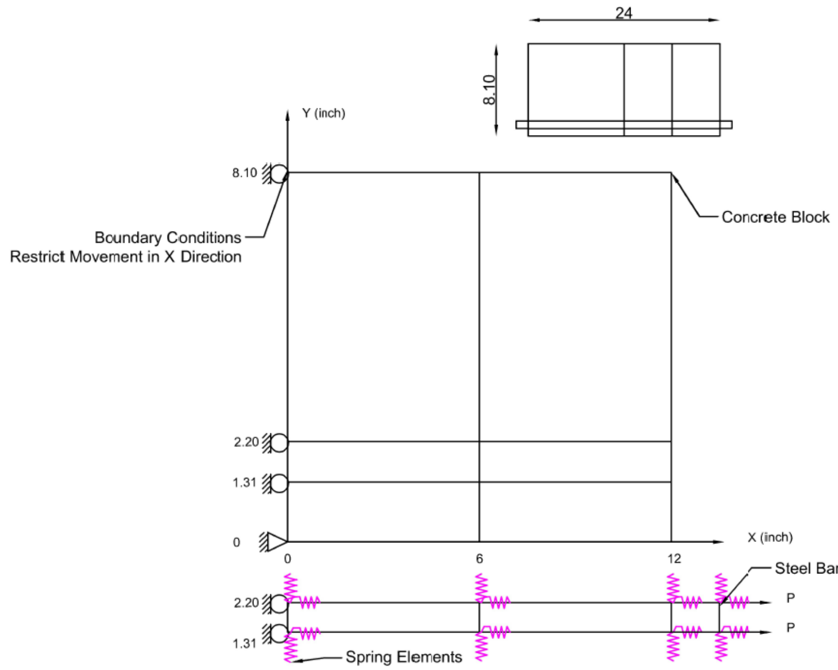

Figure 3-3 The nine-element coarse mesh for the idealization of Nielson's section is modeled in the FEMRC program.

The cracking and breakage of spring elements in each loading increment are shown in ***Figure 3-4***.

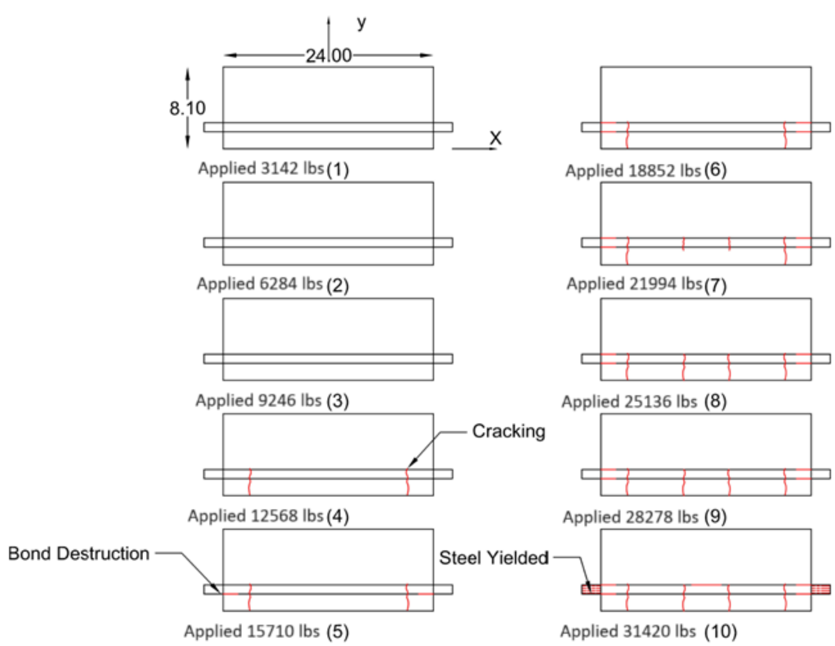

Figure 3-4 The cracking and breakage of bonds in each loading step for nine-element idealization.

Figure 3-4 shows that the bond breaks at the face of the concrete and the middle of the member, like the pattern established by Nielson (Nielson, p. 139). However, the idealization can be modified to smaller elements for more accuracy. The second idealization uses eighty-one elements. As shown in ***Figure 3-5***, the aspect ratio varies from 0.43 to 0.99.

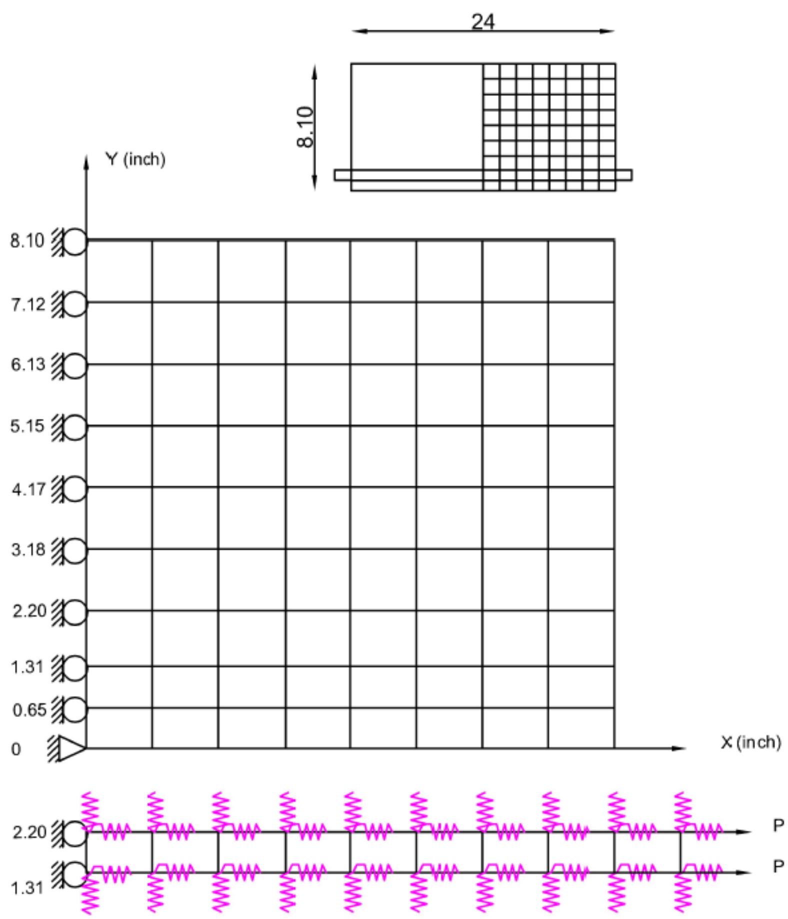

Figure 3-5 The eighty-one-element coarse mesh for the idealization of Nielson's section is modeled in the FEMRC program.

The corresponding cracks and bond breakage are shown in ***Figure 3-6***.

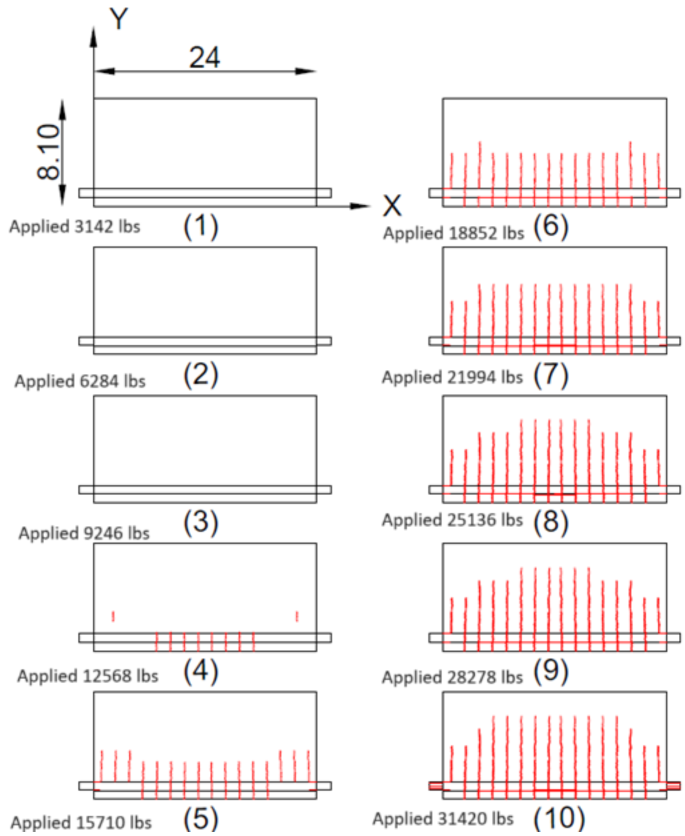

Figure 3-6 The gradual cracking and breakage of bond in each loading step for the eighty-one-element idealization.

Each load step is 4 ksi. Most of the bond between the concrete and the steel is broken at step six. After the seventh load step, or at 28 ksi, the cracks are extensive; at the final step, the steel is yielded. The final idealization models the member using 161 elements—the aspect ratio varying from 0.8 to 0.5, as shown in ***Figure 3-7***.

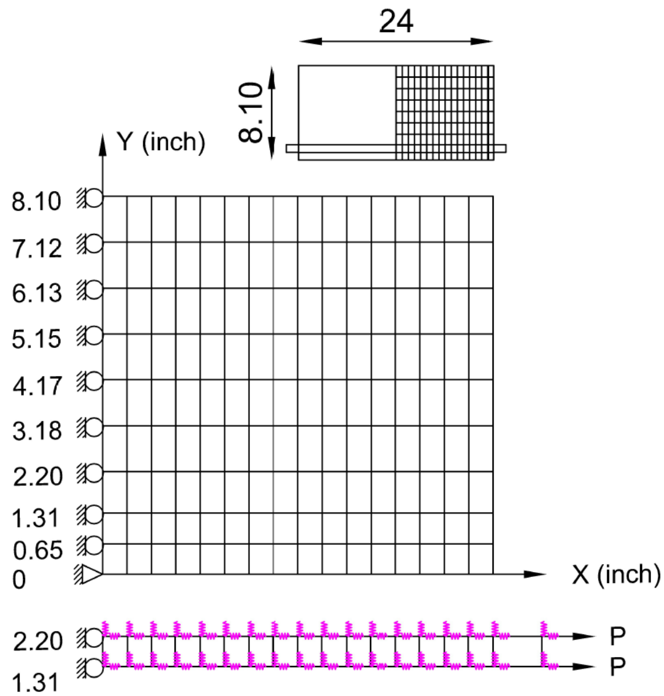

Figure 3-7 The 161-element mesh for the idealization of Nielson's section modeled in the FEMRC program.

As shown in ***Figure 3-8***, the breaking of the bond between the concrete cover and the steel bar start at the fifth stage, while part of the cover concrete near the face of the member is not broken yet. At stage seven, cracks start to appear adjacent to the concrete face, and by step nine, the concrete connected to the steel is completely crashed, and at the final step, the steel yields.

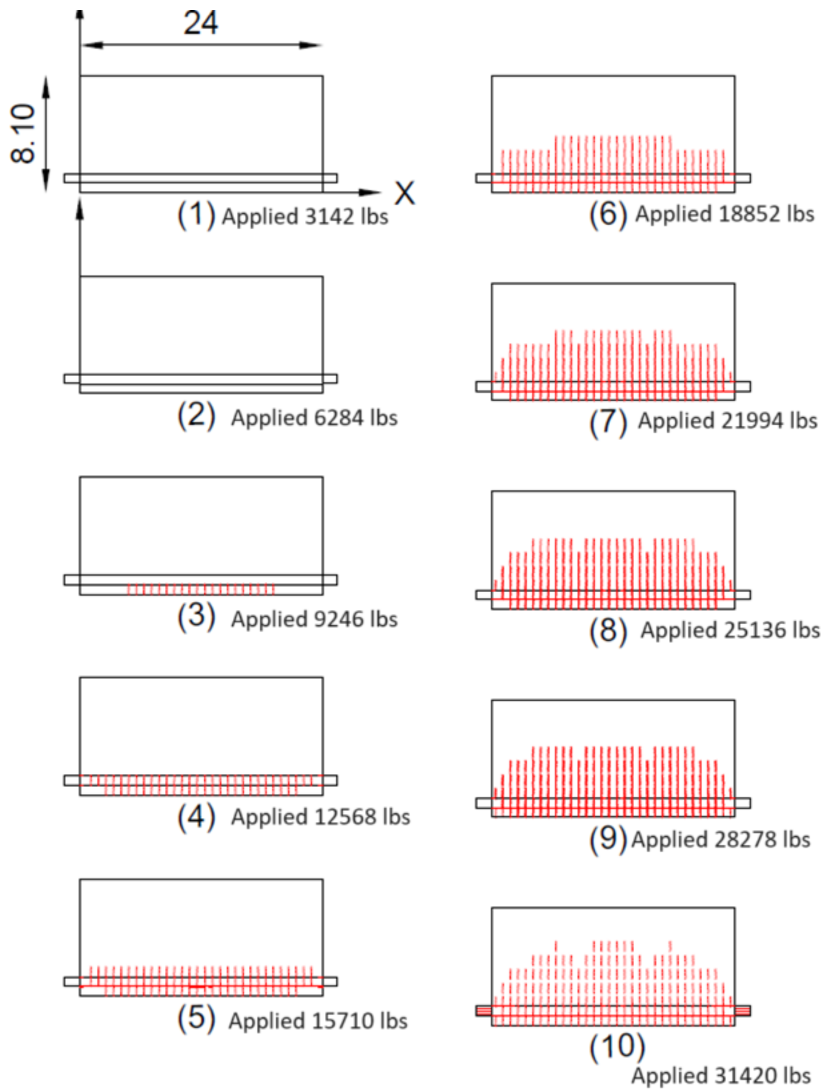

Figure 3-8 The gradual cracking and breakage of bond in each loading step for the 161-element idealization.

Nielson mentioned that the element's shape influences the accuracy of prediction. For the triangular element in his thesis, the aspect ratio of one and finer mesh gives the most truthful results (Nielson, p. 158). Thus, the stress in the last idealization will be compared to the results Nielson acquired to investigate the variation of steel stress with distance along the bar. Nielson presented a graph of curves showing steel stress along the bar for all load increments as the stress improves from zero to 40 ksi. He explained that up to 12 ksi, the bond was intact, and the steel stress was reduced from the concrete face to the concrete center. At 16 ksi, the curve leveled off at the face of the concrete because the bond failure started. At 2o, 24 and 28 ksi, the bond failure occurred at the primary crack, so the steel stress gets closer to the free-bar stress. Above 28 ksi, the bond was destroyed at the secondary crack, and thus, the free bar stress is observed (Nielson, p. 144).

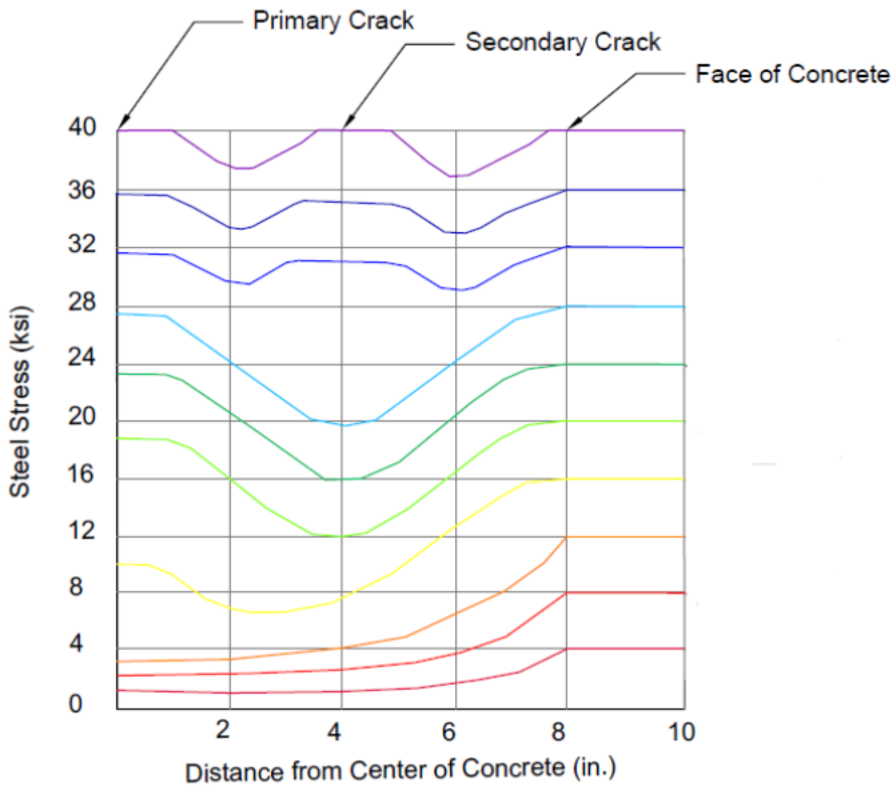

Figure 3-9 *Variation of steel stress in specimens with eccentric reinforcement* **(Nielson, p. 143)**.

Figure 3-9 shows stress variation for a 4-inch-thick prism. In this figure, from 4 ksi to 12 ksi, the concrete is not cracked, and thus, it is contributing to carrying the stresses. At the face of the concrete prism where steel is bare, distances 8 in. to 10 in., the stresses in steel are equal to applied stress. In the first three stages of loading in the middle of the concrete prism, the stresses are smaller than 4 ksi. As the concrete cracking initiates in the middle of the prism under 16 ksi stress, the stresses in steel are high but lower than the applied 16 ksi. The stresses increase with a steep slope toward the free face of the prism. This can indicate that the bond is breaking closer to the concrete face. The crack progresses in the stresses from 20 ksi to 28 ksi, and the bond breaks more in the middle of the prism and closer to the face. This is why the stress is closer to the applied stress between 0 in. and 2 in. The stress lowers between 2 in. to 6 in. distance from the middle of the prism, meaning that the bond is still working and the concrete is not cracked. In stresses larger than 28 ksi, a secondary crack forms, and steel stresses peak to the applied stress value as the cracked concrete is not contributing to support the stresses. This figure is gained from experiments on concrete prisms and is not attained by a computer program.

Figure 3-10 shows the stress along the bar for a reinforced concrete member that is 24 inches long, and the idealization consists of 161 elements. From 0 to 12 ksi, no bond breakage was observed, so the pattern of the bar stress curve can be compared to Nielson's result for the first three loadings. At 16 ksi, the FEMRC curve also levels off at the concrete face. From 20 to 28 ksi, the bond that connects the cover concrete to steel is destructed, and the bond between the top concrete and the bar is broken near the face of the concrete.

Figure 3-10 shows stress closer to free steel stress values near the concrete face, reducing at the center of the member. This diverts from the curves observed by Nielson for increments of 5, 6, and 7 ksi. The reason seems to be that in the FEMRC analysis, the top bond is not completely destroyed, and the top concrete helps distribute some of the stresses formed in steel. At stresses above 28 ksi, Nielson results show the breaking of the bond, and the steel has stresses similar to the free bar stress. However, in the analysis conducted in this thesis, the bond does not completely break until the steel yields at levels 8, 9, and 10. Thus, this part is not comparable to Nielson's result and will be neglected from this point forward.

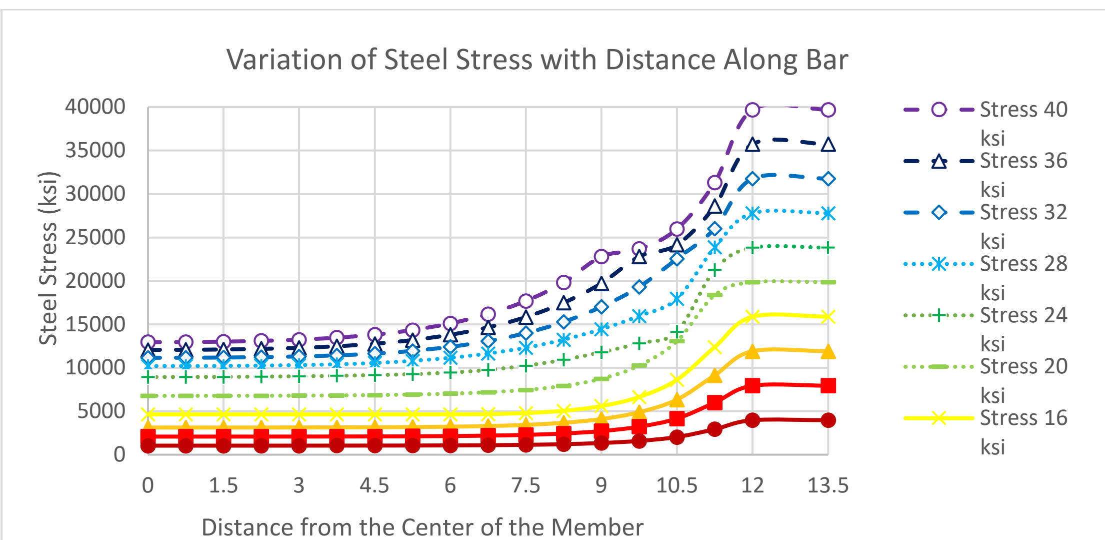

Figure 3-10 Variation of steel stress along the bar.

The steel displacement for the three-idealization analyzed by FEMRC is shown in ***Figure 3-11***. For the reasons described above, the displacement of steel for stresses higher than 22 ksi is omitted. All three analysis have the same pattern of Nielson's curve, the coarser idealizations show closer behavior to the transformed member and the finer idealization models the bond destruction better and is closer to Nielson's curve. All three analysis show that the bond is assisting the steel stress to be distributed to the concrete.

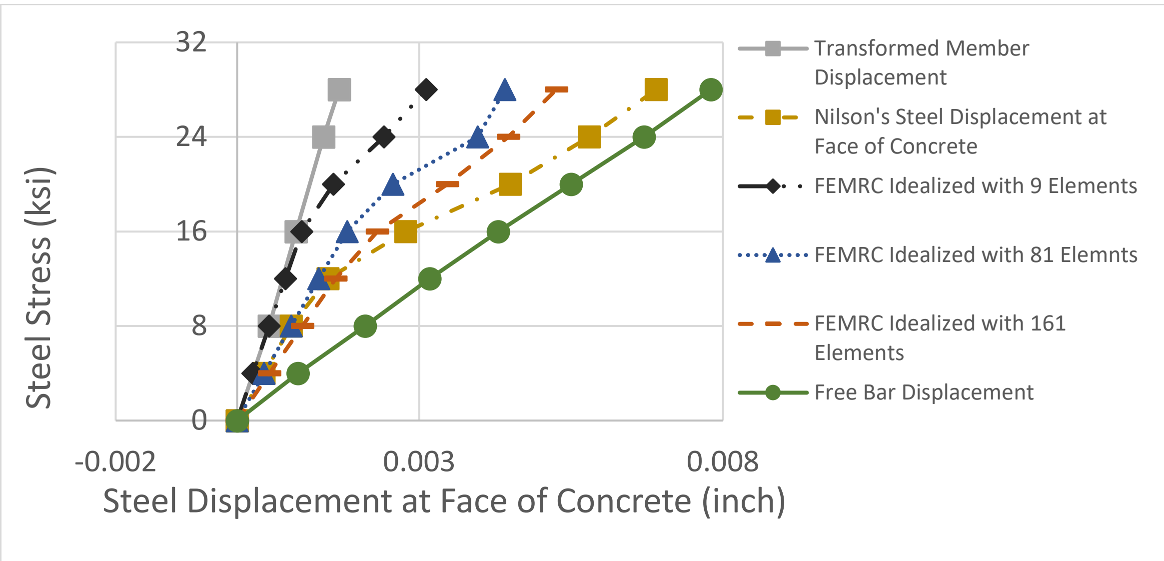

Figure 3-11　　Steel displacement for the three idealizations analyzed by FEMRC.

3-3　Conclusions:

- The bond between steel and concrete assists the stress to be transferred from steel to the concrete.
- At the location of cracks where the bond breaks steel holds stress like free steel.
- The cracked concrete that is cracked can transfer the stresses if the bond is not broken.
- After the bond breaks, the steel stress is nearly the same as the free-bar values controlled by the yield strength of the steel bar.

4- CHAPTER FOUR, MODELLING OF THE AXIAL STIFFNESS OF TRANSVERSE CONFINEMENT

In Section 2.2, the role of reinforcement in the punching shear strength of reinforced concrete was discussed with reference to the tests by Khanna et al. (2000) on a full-scale model. In this chapter, attempt is made to model the bottom transverse reinforcement of the full-scale mode.

4-1 Details of Experimental Study

The 175 mm thick deck slab of Section C of the Khanna et al. model failed under a central wheel load of 882 kN, it is noted that:

(a) the spacing of the steel girders of the model was 2.0 m;
(b) the strength of the deck slab concrete was between 30.6 and 35.0 MPa;
(c) the deck slab overhang beyond each girder was 0.75 m wide, and
(d) the wheel load was rectangular with a length of (250 cmx500 cm)

The segments were first subjected to monotonically increasing loads, peaking at approximately 200, 300, 400, 500, and 600 kN, respectively. For each load cycle, the loads were repeated until no residual deflections were observed. It is important to note that allowable wheel loads are nearly 50 KN, and the maximum observed wheel loads rarely exceed 100 kN. The applied wheel loads on the full-scale model were significantly larger than the actual wheel loads.

4-2 Idealization of a Section to Study the Behavior of Steel Inside Concrete Using Khanna et al.'s Experiment.

The following section will be idealized to test the interaction between the steel and concrete. The section is identical to Khanna et al.'s section C of his experiments. ***Figure 4-1*** shows the cross-section of the slab model.

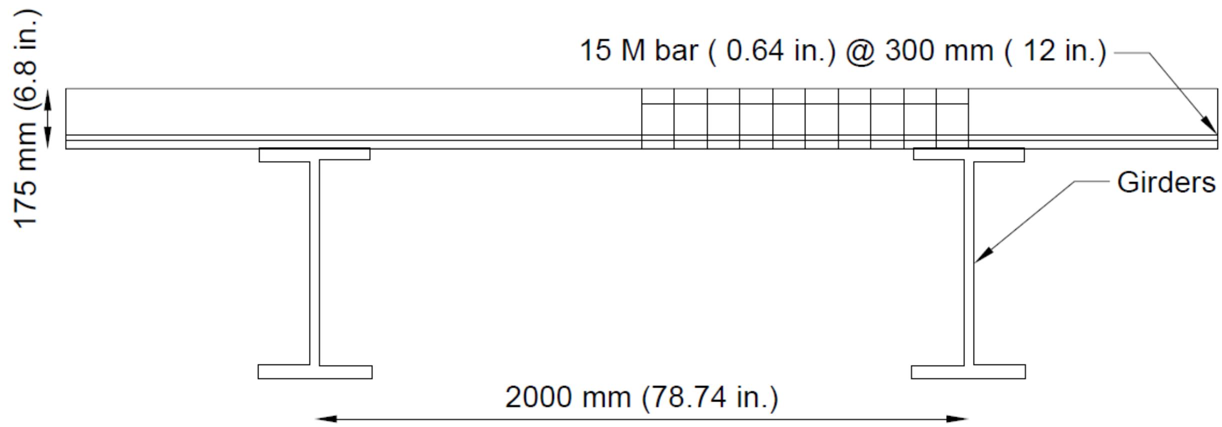

Figure 4-1 The reinforced concrete slab shows idealization in half section.

The idealized cross-section of the deck slab is shown in ***Figure 4-1*** and ***Figure 4-2***.

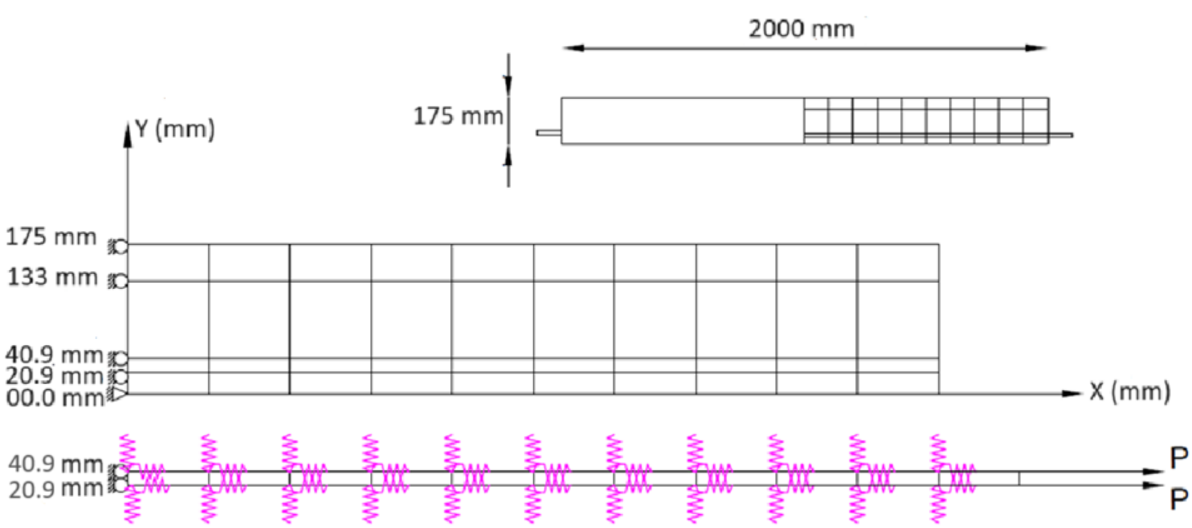

Figure 4-2 The section idealized for the FEMRC program uses 51 elements.

The idealized section shown in ***Figure 4-2*** was analyzed using the FEMRC program with tensile forces applied to the bottom transverse reinforcement. The yielding of the steel bar, breakage of bond and the development of cracks in the deck slab are shown sequentially under a load increasing in 4 ksi intervals in ***Figure 4-3***.

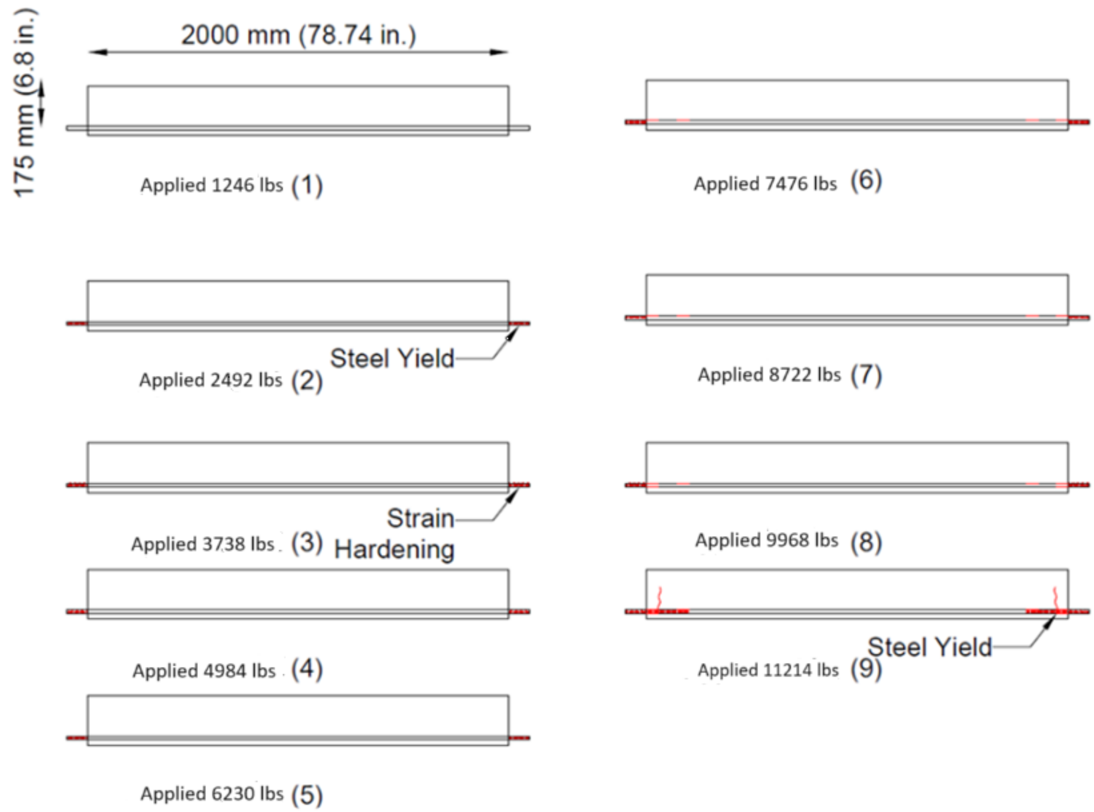

Figure 4-3 The cracking, bond breakage, and yielding of steel in the idealized section with 51 elements.

Figure 4-3 shows that the steel outside the face of concrete yields at the beginning stages of load application. In sequences (6) and (7), when the applied stresses are 24 and 28 ksi, respectively, the bond at the top of the steel near the face of the concrete breaks, and at stage (8), when the applied stress is 32 ksi, the bond at the face of concrete is broken completely. At the final stage of loading, when the applied stress is 36 ksi, two cracks in the concrete detach from the steel. The stress-displacement curve for the steel bar is shown in ***Figure 4-4***.

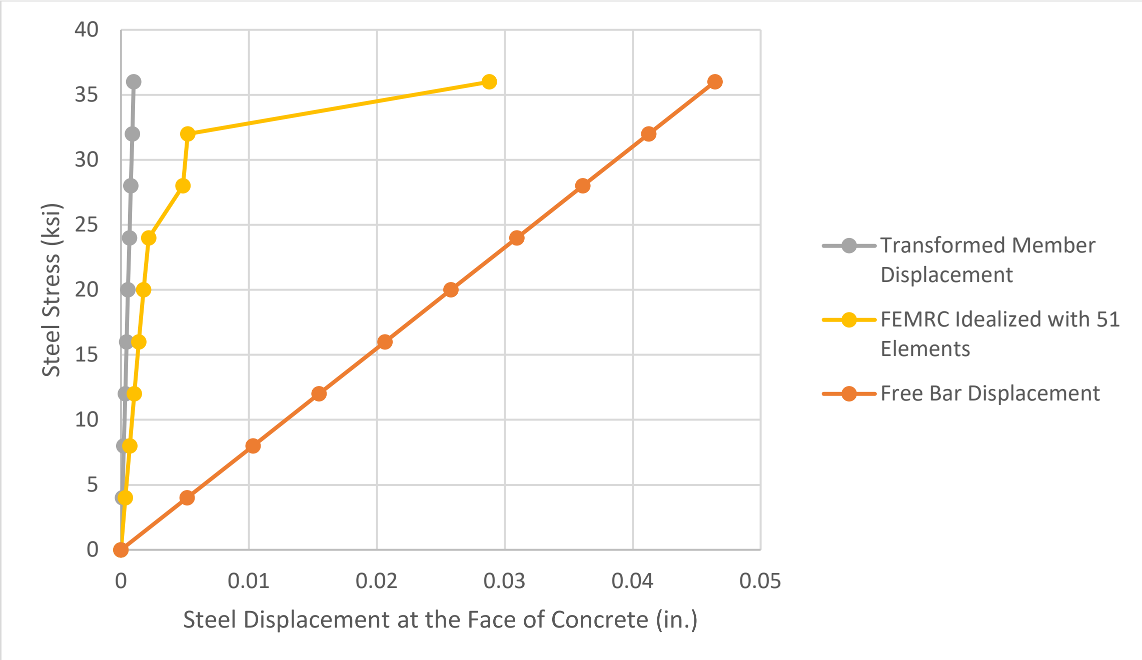

Figure 4-4 The stress-displacement curves for the steel bar

It can be seen in ***Figure 4-4*** that the behavior of the embedded steel bar is very close to that of the transformed bar, in which concrete does not crack. It is obvious that the axial stiffness of the transverse confinement in the full-scale model of the deck slab is provided by both the steel bar and un-cracked concrete.

The stress-displacement curve of the steel bar in one of the Nielson models is shown in **Figure 4.5**. It is recalled that both the cross-sections and lengths of the Nielson model were small in magnitude, because of which concrete cracked in early stages of loading and could not contribute significantly to the axial stiffness of the composite prisms.

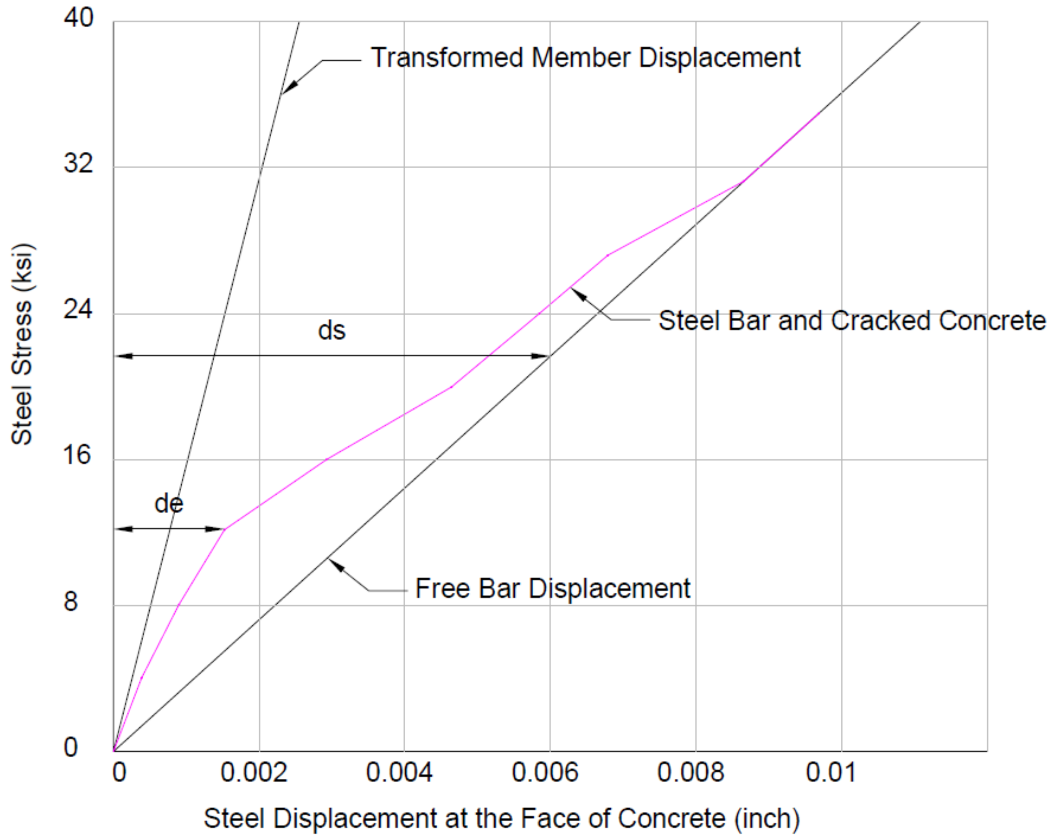

Figure 4-5 *Stress-displacement curves for one of the Nielson models of reinforced concrete prisms*

In ***Figure 4-5***, d_e is the distance of the steel bar and cracked concrete curve from the Y axle, and d_s is the distance of the free bar curve from the Y axle.

The equivalent area of steel can be calculated as

$$A_e = A_s \frac{d_s}{d_e}$$

Equation 4-1

As is the cross-sectional area of the original steel bar used, and A_e is the conceptual cross-sectional area of an imaginary bar in which the contribution of concrete is considered.

And accordingly, the diameter of the equivalent steel bar can be calculated as:

$$D_e = \sqrt{\frac{A_e \times 4}{\pi}}$$

Equation 4-2

Section C of the full-scale model with 65 elements, shown in ***Figure 4-6***., was analyzed under gradually increasing load by the FEMRC program. The crack pattern, bond breakage, and yielded elements under various stages of loading are shown in ***Figure 4-7***.

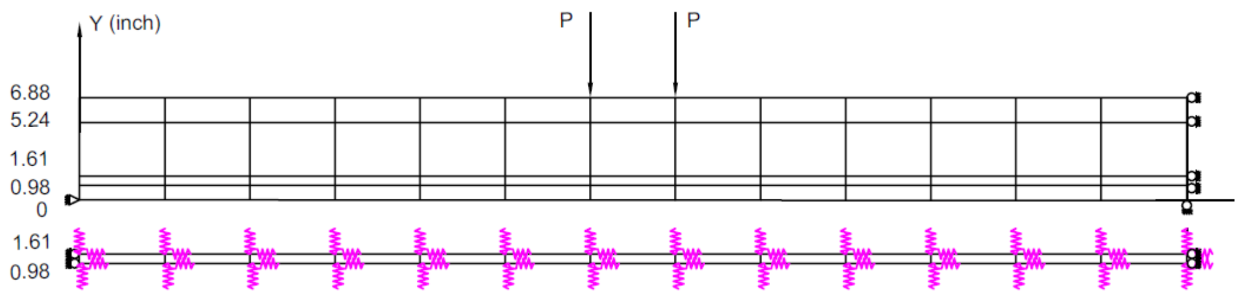

Figure 4-6 Idealization of Section C of the full-scale model for FEMRC program using 65 elements.

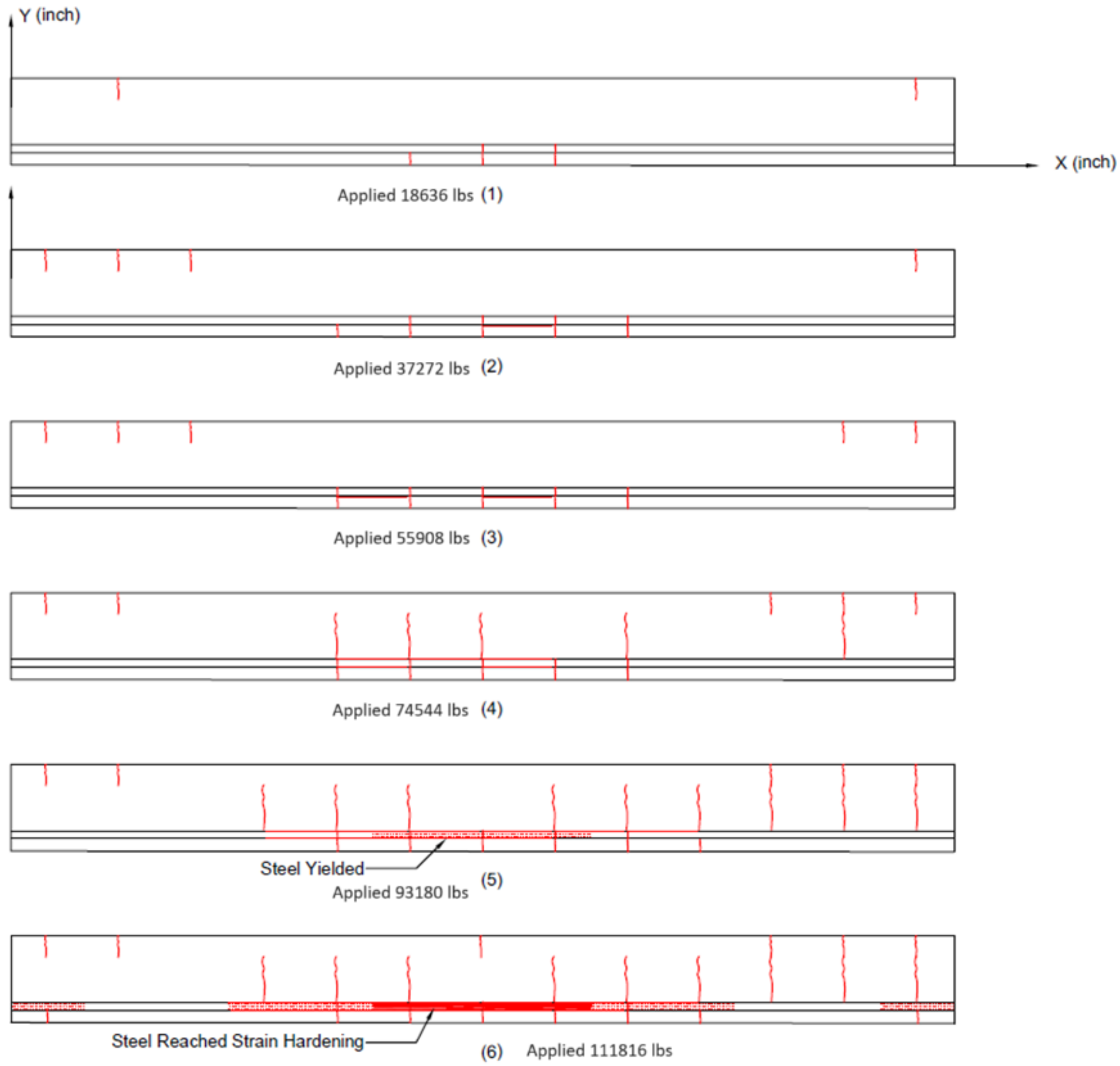

Figure 4-7 The crack pattern, broken spring elements, and yielded elements in the FEMRC idealization using 65 elements.

The crack pattern is shown in ***Figure 4-7*** is attained from the FEMRC program and shows a bending behavior as FEMRC can not model the arch action, while in the experimented deck, the failure was a punch failure with the arch action active.

As shown in ***Figure 4-8*** FEMRC can not predict the failure load as the true failure load under the formation of the arch is higher than what can be predicted by flexural failure calculation in FEMRC. So ***Figure 4-8*** does not intend to compare the failure load.

PUNCH program is based on modeling the arch and a punch failure, so the purpose of changing the punch program is to predict the punch failure load while arching occurs in the internally reinforced bridge deck slab clarifies.

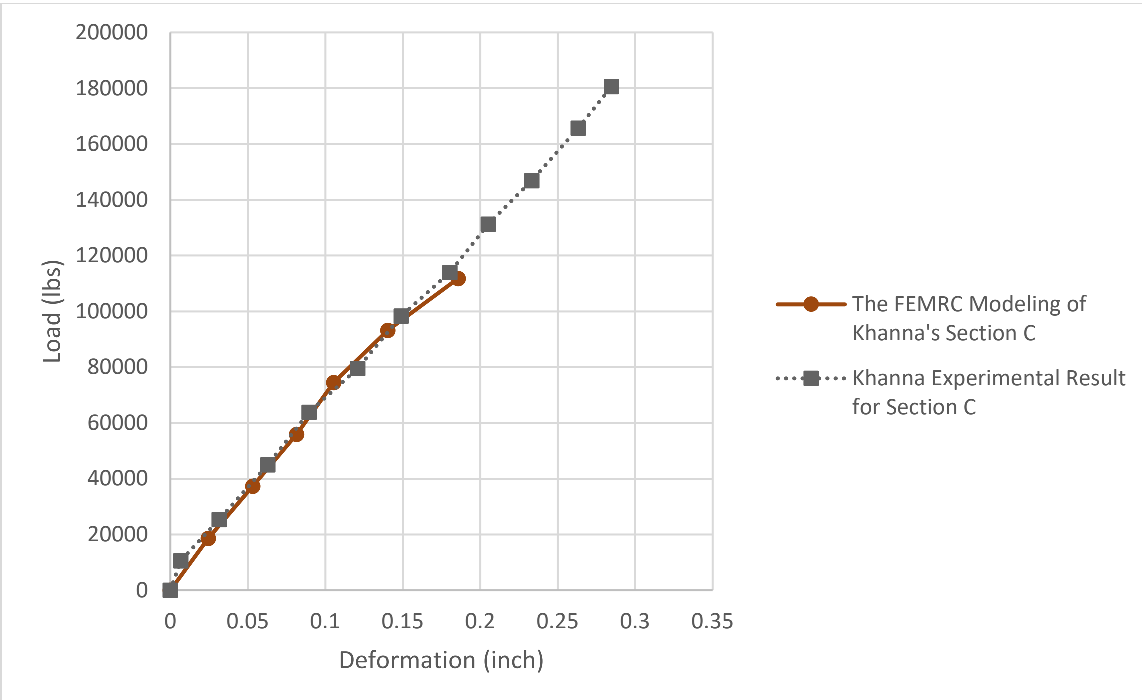

Figure 4-8 *The load-deflection curve for Section C of the full-scale model compared with the results of the FEMRC program.*

The FEMRC analysis was repeated by increasing the deck slab thickness from 175 mm to 225 mm, the minimum deck slab thickness required by the CHBDC for deck slabs in harsh environments. The idealization of the thicker deck slab is shown in ***Figure 4-9***.

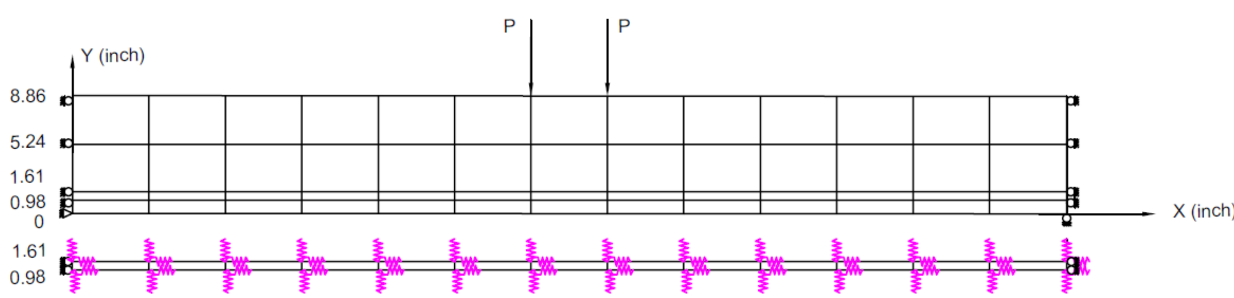

Figure 4-9 The idealization for deck slab with a thickness of 225 mm

The cracks, broken bonds, and yielded steel for the above-idealized section are shown ***Figure 4-9***, and the crack pattern, bond breakage, and yielded elements under various stages of loading are shown in ***Figure 4-10***.

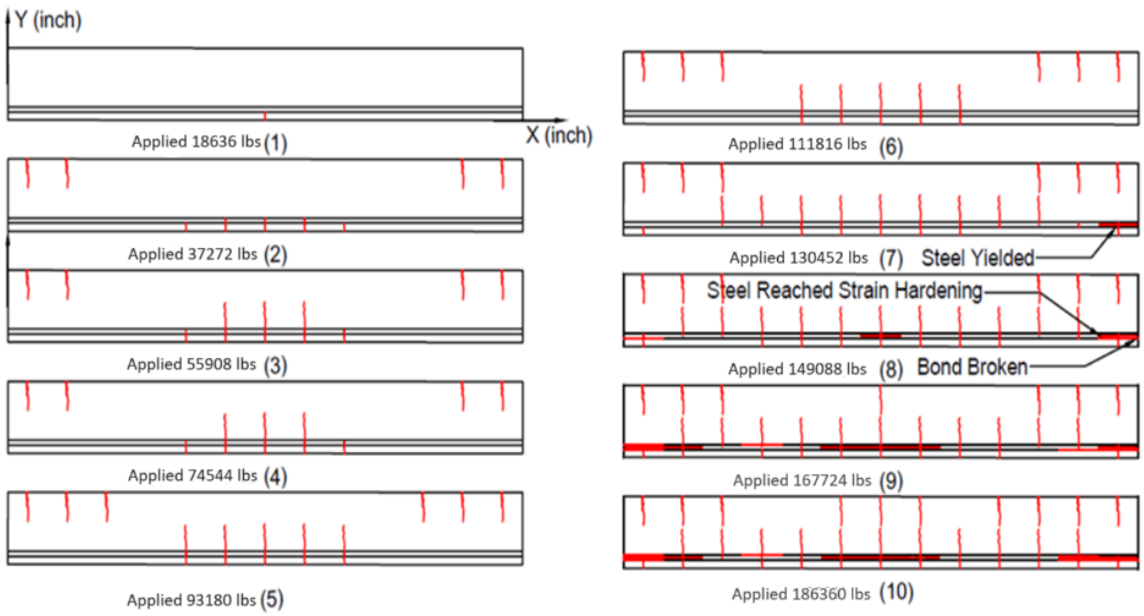

Figure 4-11 Crack pattern, bond breakage, and yielded steel for the FEMRC model of the deck slab with the thickness of 225 mm

The load-deflection curve predicted by FEMRC for the 225 mm thick deck slab are compared in **Figure 4-12** with the observed deflection for the 175 mm thick deck slab. It can be concluded from this figure that the increase in the deck slab thickness significantly increases the axial stiffness of the transverse confinement.

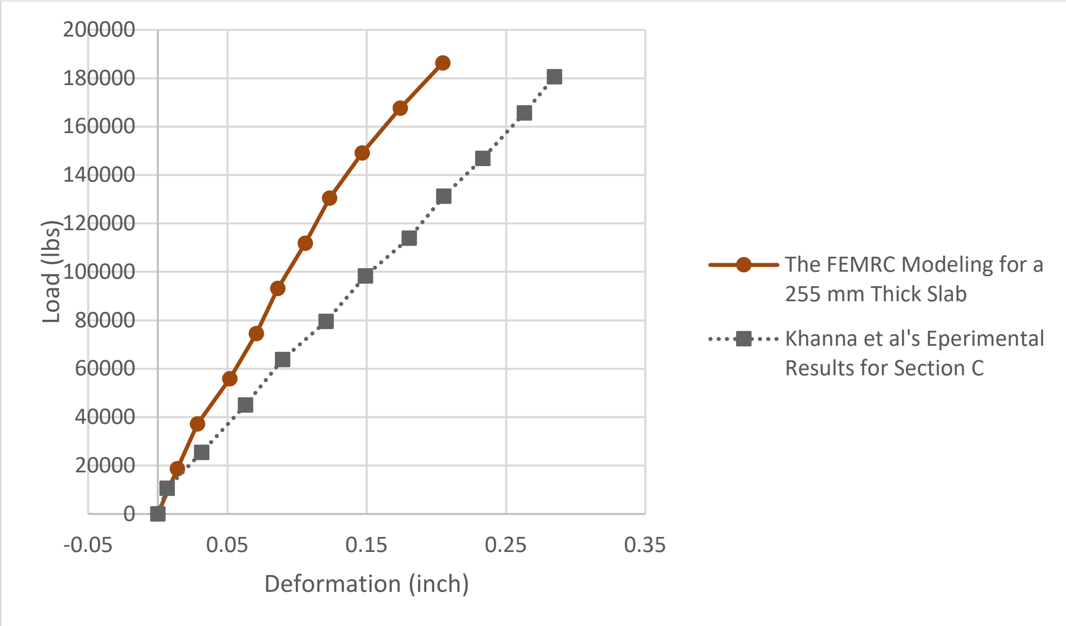

Figure 4-12 Load-deflection curves for 175 and 225 mm deck slabs

4-3 Conclusion:

Section C of the full-scale model of Khanna et al. (2000) was analyzed by the FEMRC program, and it was found that the FEM predictions compare favorably with the experimental results; however, because the FEMRC can not model the arching effect, it cannot predict the failure load as observed in experiments.

5- CHAPTER FIVE, APPLICATION OF HYPOTHETICAL EQUIVALENT DIAMETER IN PUNCH

5-1 General

The PUNCH program is a program based on equilibrium equations that take the geometry of the deck slab and the reinforcement, the magnitude of the applied load, and the material strength parameters to predict the failure load. It has been shown to accurately predict the failure load for externally reinforced bridge slabs that fail in punching shear. This program, using the given equations, lacks the ability to model any bond between steel and concrete. The formulation for PUNCH takes stiffness as an input instead, which is adequate for the design of steel-free slabs. However, when the concrete deck slab has embedded reinforcement, the bond between the steel and concrete is known to affect the slab's failure load. Through experiment and numerical modeling, load-displacement curves were acquired, proving that the bond of steel with concrete increases its stiffness. So, if the PUNCH program is to be used to design internally reinforced deck slabs, the stiffness formulation needs to be developed. *Equation 2-12* shows the existing stiffness formulation. The effect of cracked concrete resisting the steel bar and the idea of the equivalent diameter was explained earlier. The question arises: What is the magnitude of the equivalent diameter? To answer this question, the PUNCH program is used for the original bar diameter and various equivalent diameters, keeping all other inputs identical to Khanna et al.'s experiment to find the equivalent diameter that can give the experimental load-displacement results. It should be noted that the PUNCH program used in this thesis has not been modified to calculate the failure load for internally reinforced bridge deck slabs. So, it considers the internal bar an external strap using an equivalent diameter that can resemble the concrete's contribution.

5-2 The Input Parameters for the PUNCH Program and Analysis Results.

For an externally restrained deck slab, the following input is required for the PUNCH program.

- Spacing of girders: 78.7 in. (2000 mm)
- Diameter of equivalent circle for load: 18.8 in. (477.5 mm)
- Maximum compressive strength of concrete: 4351.1 psi (30 MPa)
- Elastic axial stiffness of a strap: 19486 psi (134 MPa)

- Strap to load spacing: 0.000
- Depth of slab: 6.88 in. (175 mm)
- Beta to define rectangular stress block: 0.850
- Concrete constant used for confinement: 10.000
- Area of load patch: 193.75 in^2. (125000.0 mm^2)
- Yield strain: 0.00132

For the equivalent diameters, the elastic axial stiffness is as shown in Table 1.

Table 1 The axial stiffness regarding each equivalent diameter used in the PUNCH program.

Equivalent diameter	Axial stiffness calculated using ***Equation 2-12***
1.5 D_s	(43.728 ksi) or 301.5 Mpa
2 D_s	(77.754 ksi) or 536.1 Mpa
2.1 Ds	(85.731 ksi) or 591.1 Mpa
2.4 D_s	(12.149 ksi) or 837.7 Mpa

The load-displacement curve observed in the experiment by Khanna et al. is compared in ***Figure 5-2*** with the PUNCH program results for various equivalent diameters.

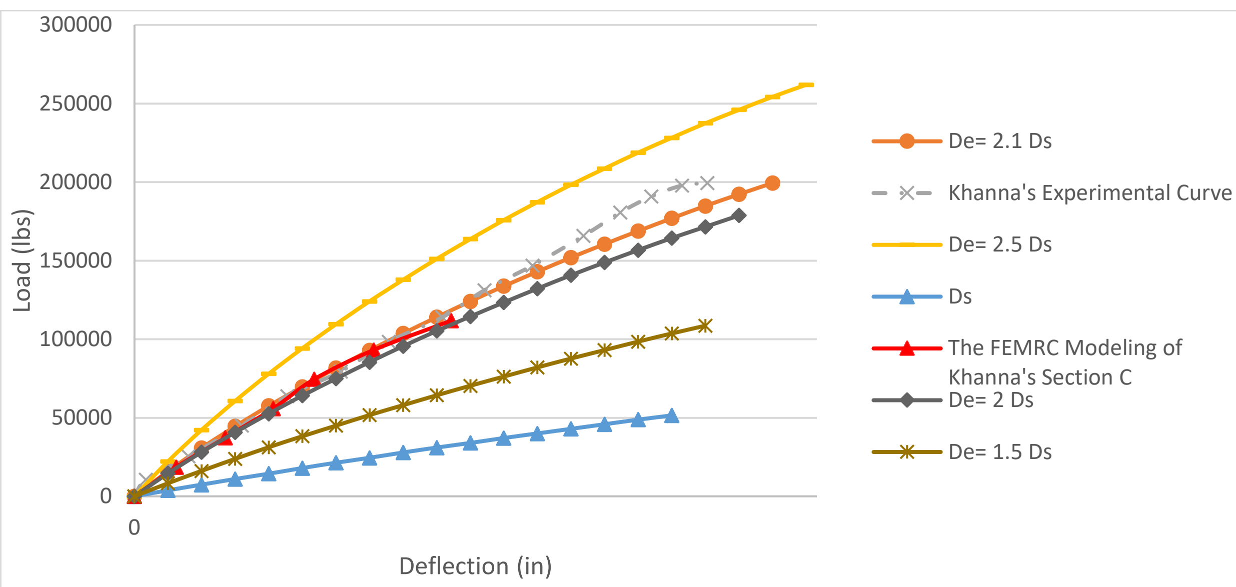

Figure 5-1 Load-deflection curves for various equivalent diameters using the PUNCH program compared to Khanna et al.'s test results for the section.

The graph shows that the equivalent diameter matches well with the diameter 2.1 times the diameter of the reinforcing bar. The FEMRC is assuming flexural failure in modeling the deck slab, so the FEMRC result shown in ***Figure 5-1*** does not represent the failure load in punch mode.

Also, in ***Figure 5-1*** At this stage, the best matching equivalent diameter is found by try-and-error of different diameters. So, the failure loads shown are to resemble the concrete contribution.

The same graph can be drawn for the imaginary section with a slab thickness of 225 mm, described in ***Figure 4-9***.

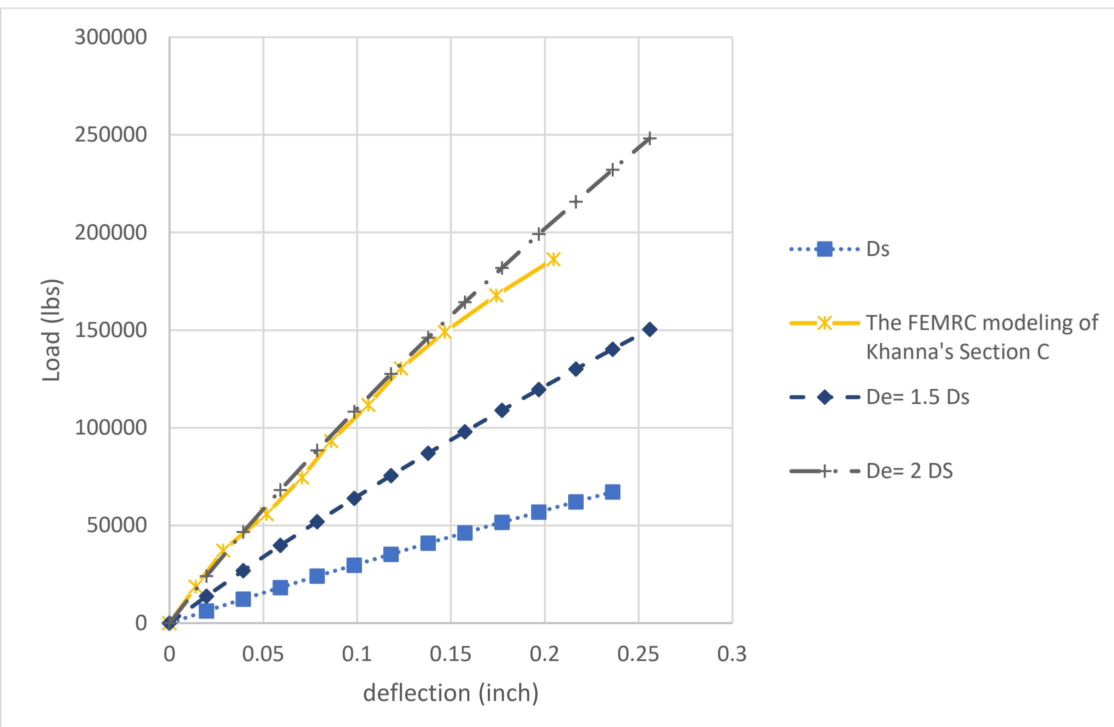

Figure 5-2 Load-deflection curve for equivalent diameters using the PUNCH program compared to FEMRC results for the assumed section.

The results show that the equivalent diameter of 2 times the cross-sectional diameter of the reinforcement should be used in the PUNCH program.

Referring to ***Figure 3-1*** The slope of the stress displacement figure shows the stiffness; Nielson's experiment results show a change of slope as the stresses progress, which means the stiffness changes due to the change of concrete contribution. So, the PUNCH program should be modified to take in new stiffness using the idea of equivalent diameter as the load increases.

5-3 Conclusions:

The cracked concrete and steel interact with embedded reinforcement in a concrete bridge deck slab. This linkage between concrete and steel results in the composite of both materials having a stress-deflection behavior between the intact concrete and the bar free from concrete. The FEM can use spring elements to model the bond. However, FEMRC lacks the capability to model punch failure and predict the real failure load.

In the equations that define punching failure in reinforced concrete, used in the PUNCH program, the contribution of concrete could be reflected in the stiffness formula.

The findings of this study indicate that when performing a rational analysis of an internally reinforced bridge deck slab with a conventional cross-section and material, the stiffness equation needs to be adjusted. Specifically, the diameter of the steel should be replaced with an equivalent bar diameter. This is necessary to account for the effect of concrete surrounding the steel.

6- CHAPTER SIX, FUTURE RESEARCH

The hypothetical equivalent diameter can be encoded in the definition of stiffness for the PUNCH program such that it alters accordingly for each increment of loading. The program then can be verified with the experiment results of real size deck slabs tested to failure. The new program will be called PUNCH-ED to represent Equivalent Diameter.

Currently the FEMRC program analyses members in two dimensions. The main focus of analysis has been on the two-dimensional modeling of deck slabs. As previously discussed, the slab should be restrained longitudinally and transversally and the interaction between the slab and supports should be investigated in three dimensions. The 3-D finite element modeling can be used to develop the 3D-FEMRC program.

References:

American Institute of Steel Construction, 2022. *Steel Bridge Design Handbook.* s.l.:AISC2022.

Bakht, B., (1996). *Revisiting Arching in Deck Slabs.* s.l.:Canadian Journal of Civil Engineering.

Bakht, B., 1996. *Revisiting Arching in Deck Slabs.* s.l.:Canadian Journal of Civil Engineering.

Canadian Standard Association, (2006). *Canadian Highway Bridge Design Code.* s.l.:Canadian Standard Association.

Canadian Standard Association, 2006. *Canadian Highway Bridge Design Code.* s.l.:s.n.

Hewitt, B. E.; Batchelor, B. de V., (1975). Punching Shear Strength of Restrained Slabs. *Journal of the Structural Division,* pp. 1837-1853.

Hewitt, Brian E.; Batchelor, Barrington de V., 1975. Punching Shear Strength of Restrained Slabs. *Journal of the Structural Division,* pp. 1837-1853.

Hewitt, B. E., (1972). *An Investigation of Punching Strength of Restrained Slabs with Particular Preference to the Deck Slabs of Composite I-Beam Bridges.* Kingston: Department of Civil Engineering Queen's University at Kingston.

Hewitt, B. E., 1972. *An Investigation of Punching Strength of Restrained Slabs with Particular Preference to the Deck Slabs of Composite I-Beam Bridges.* Kingston: Department of Civil Engineering Queen's University at Kingston.

Khanna, S., Mufti, A. & Bakht, B., (2000). *Experimental Investigation of the Role of Reinforcement in the Strength of the Concrete Deck Slabs.* s.l.:Canadian Journal of Civil Engineering.

Khanna, S., Mufti, A. & Bakht, B., 2000. *Experimental Investigation of the Role of Reinforcement in the Strength of the Concrete Deck Slabs.* s.l.:Canadian Journal of Civil Engineering.

Kinuenen, S. & Nylander, H., 1969. *Punching of the Concrete Slab without Shear Reinforcement..* Stockholm: Transaction of the Royal Institute of Technology.

Lyu, Y., 2022. *Finite Element Method, Element Solutions.* Dalian, Liaoning, China: Springer.

Mufti, A., Bakht, B. & Jaeger, L., (2008). *Recent Advances in Bridge Engineering.* s.l.:JMBT Structures Research Inc..

Mufti, A., Bakht, B. & Jaeger, L., 2008. *Recent Advances in Bridge Engineering.* s.l.:JMBT Structures Research Inc..

Mufti, A. & Newhook, J., 1995. *Punching Shear Strength of Restrained Concrete Bridge Deck Slabs.* s.l.:ACI Structural Journal.

Mufti, A. & Newhook, J., 1998. *Punching Shear Strength of Restrained Concrete Bridge Deck Slabs.* s.l.:ACI Structural Journal.

Mufti, A., Newhook, J. & Khanna, O., n.d. *Predicting the Punching Behavior of Reinforced Concrete Bridge Decks.* s.l.:General Conference Structural Engineering.

Mufti, Mirza, McCutheon & Houde, 1970. *A Study of the Behaviour of Reinforced Concrete Elements Using Finite Elements,* s.l.: Structural Concrte Series No. 70-5.

Mufti, Newhook & Tadros, 2008. *PUNCH User Manual,* Winnipeg: ISIS Candada Research Network University of Manitoba.

Newhook, J. & Mufti, A., n.d. *Steel-Free Concrete Bridge Deck the Salmone River Project: Experimental Verification.* s.l.:s.n.

Newhook, J. P., 1997. *The Behavior of Steel-Free Concrete Deck Slabs Under the Static Loading Condition.* Halifax, Nova Scotia: Technical University of Nova Scotia.

Nielson, A. H., (1967). *Finite Element Analysis of Reinforced Concrete, PhD thesis, University of California, Berkeley, California, USA.* Berkely, California: University of California.

Spokowski, R. W., May 1972. *Finite Element Analysis of Reinforced Concrete Member.* Montreal: Department of Civil Engineering and Applied Mechanics McGill University.